nature methods

ARTICLES

https://doi.org/10.1038/s41592-018-0232-7

Corrected: Author Correction

A pH-correctable, DNA-based fluorescent reporter for organellar calcium

Nagarjun Narayanaswamy[1,2,4], Kasturi Chakraborty[1,2,4*], Anand Saminathan[1,2], Elizabeth Zeichner[1], KaHo Leung[1,2], John Devany[3] and Yamuna Krishnan[1,2*]

It is extremely challenging to quantitate lumenal Ca^{2+} in acidic Ca^{2+} stores of the cell because all Ca^{2+} indicators are pH sensitive, and Ca^{2+} transport is coupled to pH in acidic organelles. We have developed a fluorescent DNA-based reporter, *CalipHluor*, that is targetable to specific organelles. By ratiometrically reporting lumenal pH and Ca^{2+} simultaneously, *CalipHluor* functions as a pH-correctable Ca^{2+} reporter. By targeting *CalipHluor* to the endolysosomal pathway, we mapped lumenal Ca^{2+} changes during endosomal maturation and found a surge in lumenal Ca^{2+} specifically in lysosomes. Using lysosomal proteomics and genetic analysis, we found that *catp-6*, a *Caenorhabditis elegans* homolog of ATP13A2, was responsible for lysosomal Ca^{2+} accumulation—an example of a lysosome-specific Ca^{2+} importer in animals. By enabling the facile quantification of compartmentalized Ca^{2+}, *CalipHluor* can expand the understanding of subcellular Ca^{2+} importers.

Ca^{2+} regulates diverse cellular functions upon its controlled release from different intracellular stores that initiate signaling cascades[1,2]. Lysosomes have recently been recognized as 'acidic Ca^{2+} stores', and lumenal Ca^{2+} is central to diverse functions[3]. Lysosome function is particularly important in neurons given the preponderance of lysosome-related genes in diverse neurological disorders, including ~60 lysosomal storage disorders[4]. For example, risk genes for Parkinson's disease, such as LRRK2, ATP6AP2, ATP13A2, and the genetic-risk-associated *GBA1* gene, are predicted to act in lysosomal pathways[5].

Although electrophysiology has enabled the discovery of several channels that release lysosomal Ca^{2+}, mediators of lysosomal Ca^{2+} import have not yet been identified[3,6]. Lysosomal Ca^{2+} release channels are amenable to investigation because Ca^{2+} release can be tracked using cytosolic Ca^{2+} dyes or genetically encoded Ca^{2+} indicators anchored to the cytoplasmic face of the lysosome[7–9]. On Ca^{2+} release, these probes indicate cytosolic Ca^{2+} in the area surrounding lysosomes. In contrast, lumenal Ca^{2+} cannot be quantitated, impeding the study of lysosomal Ca^{2+} importers. Consequently, lysosomal Ca^{2+} importers have not yet been identified in animals[10], with the closest evidence being that the *Xenopus* CAX gene localizes in lysosomes on overexpression[11].

The inability to quantify Ca^{2+} in acidic organelles arises because all Ca^{2+} indicators function by coordinating Ca^{2+} through carboxylate groups that get protonated at acidic pH[12]. This changes probe affinity to Ca^{2+} ions. Further, organellar pH is coupled to the entry and exit of lumenal Ca^{2+} (ref. [13]). Thus, it is non-trivial to deconvolute the contribution of Ca^{2+} to the observed fluorescence changes of any Ca^{2+} indicator. Previous attempts used endocytic tracers bearing either pH- or Ca^{2+}-sensitive dyes[13–17] or fluorescent-protein-based sensors[18] to serially measure population-averaged pH and apparent Ca^{2+} in different batches of cells, thus scrambling information from individual endosomes. Given the broad pH distribution in endocytic organelles, this approach does not provide the resolution needed to study Ca^{2+} import[19].

Here we used a combination reporter for pH and Ca^{2+} to map both ions in parallel in the same endosome with single-endosome addressability, achieving highly accurate measurements of lumenal Ca^{2+}. Using the pH reporter module of the combination reporter, we deduced the pH in individual endosomes. By knowing exactly how the affinity of the Ca^{2+}-sensitive module, its dissociation constant K_d, changes with pH, we were able to apply a K_d correction factor suited to the lumenal pH of each endosome to thereby compute the true value of lumenal Ca^{2+} with single-endosome resolution.

DNA nanodevices are versatile chemical reporters that can quantitatively map second messengers in real time, in living systems[20–23]. The modularity of DNA allows us to integrate distinct functions in precise stoichiometries into a single assembly. These include (1) a module to fluorescently sense a given ion, (2) a normalizing module for ratiometric quantitation, and (3) a targeting module to localize the reporter in a specific organelle[20]. We have thus measured H^+ and Cl^- in endocytic organelles[21–25]. Here we describe the use of a DNA-based fluorescent reporter, *CalipHluor*, to quantitatively map organellar pH and Ca^{2+} simultaneously and with single-organelle addressability. *CalipHluor* comprises four modules: a pH-sensitive module, a Ca^{2+}-sensitive fluorophore, an internal reference dye to ratiometrically quantitate pH as well as Ca^{2+}, and a targeting domain to transport *CalipHluor* to a specific organelle.

By targeting *CalipHluor* to the scavenger receptor-mediated endocytic pathway, we mapped lumenal Ca^{2+} as a function of endosomal maturation in nematodes. We found that Ca^{2+} concentration is fairly low in early and late endosomes, but undergoes an ~35-fold surge in lumenal Ca^{2+} in lysosomes, thus implicating the existence of lysosome-specific Ca^{2+} import mechanisms. We identified the P5 ATPase ATP13A2 as a potential candidate given its similarity to a well-known Ca^{2+} importer in the endoplasmic reticulum[26]. ATP13A2 transports divalent ions such as Mg^{2+}, Mn^{2+}, Cd^{2+}, and Zn^{2+}, yet has not been tested for its ability to transport Ca^{2+} (refs [27,28]). We found that the *C. elegans* homolog of ATP13A2, *catp-6*, functions in opposition to the well-known lysosomal Ca^{2+} release channel, *cup-5*[29]. We then determined that the human homolog, ATP13A2, also facilitates lysosomal Ca^{2+} entry by measuring lysosomal Ca^{2+} in fibroblasts derived from subjects with Kufor–Rakeb

[1]Department of Chemistry, The University of Chicago, Chicago, IL, USA. [2]Grossman Institute of Neuroscience, Quantitative Biology and Human Behavior, The University of Chicago, Chicago, IL, USA. [3]Department of Physics, The University of Chicago, Chicago, IL, USA. [4]These authors contributed equally: N. Narayanaswamy, K. Chakraborty. *e-mail: kasturi@uchicago.edu; yamuna@uchicago.edu

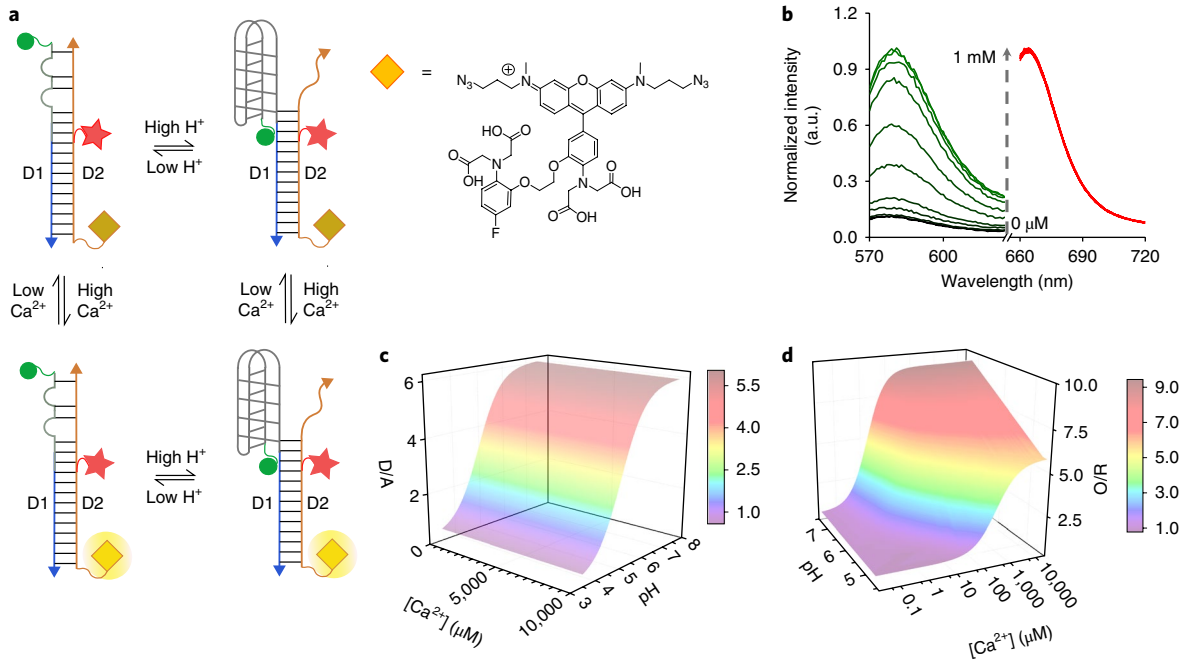

Fig. 1 | Design and characterization of *CalipHluor*$_{Ly}$. **a**, Working principle of *CalipHluor*$_{Ly}$. pH-induced FRET between Alexa Fluor 488 (donor; green sphere) and Alexa Fluor 647 (acceptor; red star) reports on pH ratiometrically. A Ca^{2+}-sensitive dye (Rhod-5F; yellow diamond; excitation maxima λ_{ex} = 560 nm) and Alexa Fluor 647 (λ_{ex} = 650 nm) report Ca^{2+} ratiometrically by direct excitation. D1 and D2 represent two complementary DNA strands. **b**, Fluorescence emission spectra of *CalipHluor*$_{Ly}$ corresponding to Rhod-5F (green) and Alexa Fluor 647 (red) with increasing [Ca^{2+}] at pH = 7.2. a.u., arbitrary units. **c**, 3D surface plot of D/A or pH response of *CalipHluor*$_{Ly}$ as a function of pH and [Ca^{2+}]. **d**, 3D surface plot of the O/R or Ca^{2+} response of *CalipHluor*$_{Ly}$ as a function of pH and [Ca^{2+}].

syndrome. This constitutes what to our knowledge is the first example of a lysosomal Ca^{2+} importer in the animal kingdom.

Results

Design and in vitro characterization of *CalipHluor*. We describe the design and characterization of a fluorescent, DNA-based combination reporter for pH and Ca^{2+} called *CalipHluor*$_{Ly}$. *CalipHluor*$_{Ly}$ is a 57-base-pair DNA duplex comprising two strands, D1 and D2, and bears three distinct domains (Fig. 1a and Supplementary Table 1). The first domain in *CalipHluor*$_{Ly}$ is a Ca^{2+}-reporter domain that uses a novel small molecule that functions as a Ca^{2+} indicator that we denote Rhod-5F[30]. Rhod-5F consists of a 1,2-bis(oaminophenoxy) ethane-N,N,N′,N′-tetraacetic acid (BAPTA) core, a rhodamine fluorophore (λ_{ex} = 560 nm; λ_{em} = 580 nm), and an azide linker. In the absence of Ca^{2+}, the rhodamine fluorophore in Rhod-5F is quenched by photoinduced electron transfer from the BAPTA core. On Ca^{2+} chelation, quenching is relieved, resulting in high fluorescence. Note that protonation of the amines in BAPTA also relieves photoinduced electron transfer[12]. Thus, the percentage change in signal as well as the K_d of Rhod-5F will be affected by pH. The K_d of Rhod-5F for Ca^{2+} binding is indeed pH dependent, as shown in the Supplementary Fig. 1.

Rhod-5F is attached to the D2 strand bearing a dibenzocyclooctyne (DBCO) group by click chemistry[31]. Conjugation to D2 did not change the K_d of Rhod-5F in *CalipHluor*$_{Ly}$ (Fig. 1b). In *CalipHluor*$_{Ly}$, Rhod-5F (orange; O) shows a K_d of 1.1 μM at pH 7.2 that increases as acidity increases.

For ratiometric quantification of Ca^{2+} we incorporate Alexa Fluor 647 as a reference dye (λ_{ex} = 630 nm; λ_{em} = 665 nm) on *CalipHluor*$_{Ly}$, positioned so that it does not induce fluorescence resonance energy transfer (FRET) with Rhod-5F. Alexa Fluor 647 was chosen for its negligible spectral overlap with Rhod-5F and insensitivity to pH, Ca^{2+}, and other ions (Fig. 1a). The fixed stoichiometry of Alexa Fluor 647 efficiently corrects for Rhod-5F intensity changes due to inhomogeneous probe distribution in cells, thus making the ratio of Rhod-5F (O) and Alexa Fluor 647 (red; R) intensities in *CalipHluor* probes proportional only to pH and Ca^{2+}. The second domain (gray line) constitutes a DNA-based pH-reporter domain that we have previously described, called the *I-switch*[21] (Fig. 1a). This *I-switch* has been used to map pH in diverse endocytic organelles in living cells[21–25]. To map pH in early and late endosomes we made *CalipHluor*, a variant suited to the weaker acidities in these organelles (Supplementary Table 1 and Supplementary Fig. 2c). *CalipHluor* and *CalipHluor*$_{Ly}$ formation were characterized by gel electrophoresis (Supplementary Fig. 2a–e). The third 'integration' domain comprises a 30-mer duplex that integrates the pH- and Ca^{2+}-reporter domains into a single DNA assembly. One end is fused to the *I-switch* and the other is fused to the Ca^{2+} sensor. This domain also helps in targeting, because its anionic nature aids recognition and trafficking by scavenger receptors in a DNA-sequence-independent manner[22].

The response characteristics of *CalipHluor* and *CalipHluor*$_{Ly}$ were investigated as a function of pH and Ca^{2+}, and their pH- and Ca^{2+}-sensitive regimes were determined (Fig. 1c,d and Supplementary Fig. 2f,g). A three-dimensional (3D) surface plot of donor-to-acceptor ratio (D/A) as a function of pH and different values of free [Ca^{2+}] is shown in Fig. 1c. These revealed that the pH-reporting capabilities of *CalipHluor* and *CalipHluor*$_{Ly}$ are between pH 5.0–7.0 and pH 4.0–6.5 with fold changes in D/A ratios of 4.0 and 5.5, respectively (Fig. 1c and Supplementary Fig. 2g)[22]. Notably, the fold changes in D/A ratios were invariant over a range of free Ca^{2+} concentrations from 20 nM to 10 mM, showing that pH sensing by these probes is unaffected by Ca^{2+} levels (Fig. 1c).

In parallel, the intensities of Rhod-5F (O) and Alexa Fluor 647 (R) in *CalipHluor*$_{Ly}$ obtained from direct excitation yielded Rhod-5F-to-Alexa-Fluor-647 ratio (O/R) values. An analogous 3D surface plot of O/R values as a function of [Ca^{2+}] and pH showed a sigmoidal increase as a function of Ca^{2+} with an approximately nine fold

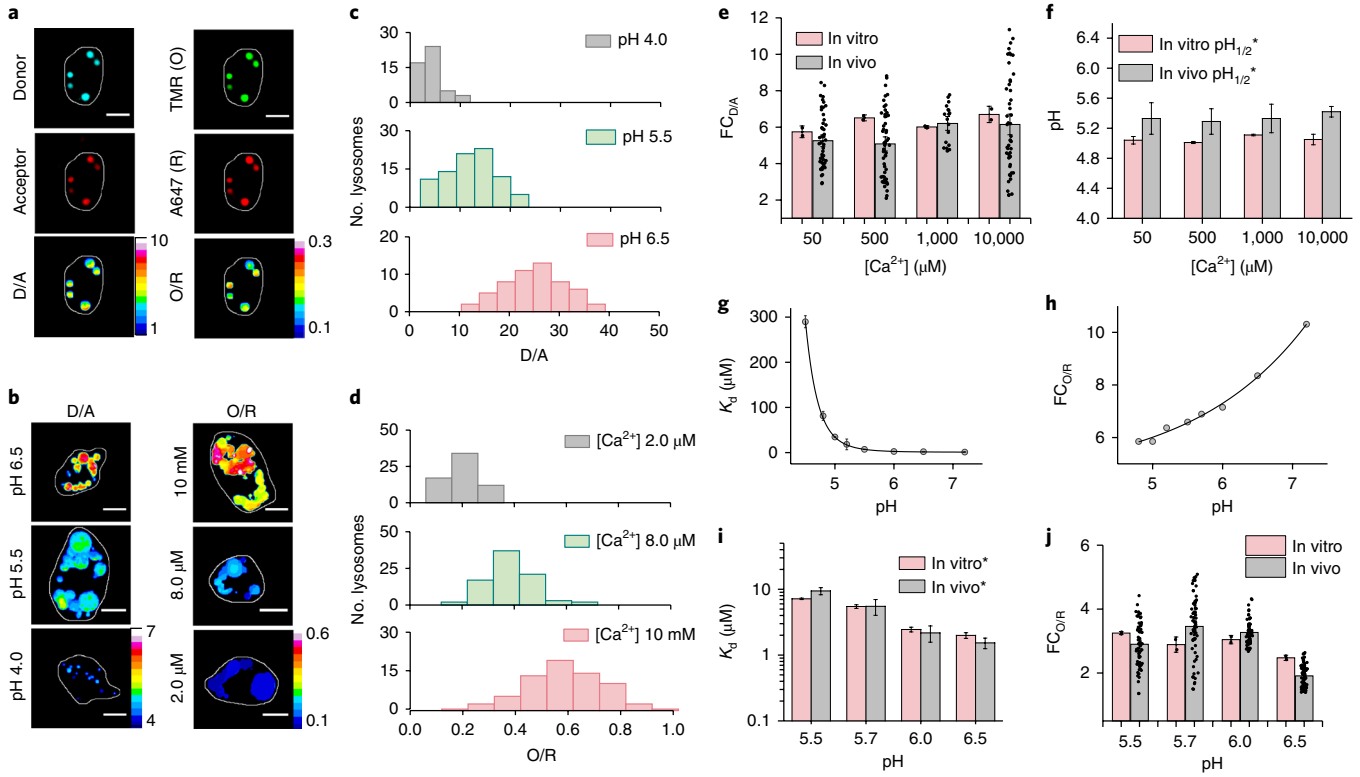

Fig. 2 | In vivo sensing characteristics of *CalipHluor*$_{Ly}$. **a**, Representative *CalipHluor*$_{Ly}$-labeled coelomocytes imaged in the donor, acceptor, Rhod-5F (TMR, O), and Alexa Fluor 647 (R) channels. D/A and O/R are the corresponding pixel-wise pseudocolor images. **b**, Representative pseudocolored D/A and O/R maps of coelomocytes clamped at the indicated pH and free [Ca^{2+}]. **c**, Distribution of D/A ratios of ≥50 endosomes clamped at the indicated pH (n = 10 cells). **d**, Distribution of O/R ratios of ≥50 endosomes clamped at different indicated free [Ca^{2+}] values (n = 10 cells). **e**,**f**, Comparison of fold change of D/A ratios from pH 4 to 6.5 (**e**) and $pH_{1/2}$ from pH 4 to 6.5 of *CalipHluor*$_{Ly}$ (**f**) at different [Ca^{2+}] values obtained in vitro (peach) and in vivo (gray). **g**,**h**, *CalipHluor*$_{Ly}$ K_d (**g**) and fold change of O/R (**h**) as a function of pH. **i**,**j**, Comparison of K_d (**i**) and $FC_{O/R}$ from 1 µM to 10 mM [Ca^{2+}] (**j**) of *CalipHluor*$_{Ly}$ at the indicated pH obtained in vitro (peach) and in vivo (gray). Scale bars, 5 µm. Data represent mean ± s.e.m. *Error is obtained from the non-exponential fit. Experiments were repeated thrice independently with similar results.

change in O/R at pH 7.2 (Fig. 1d). At lysosomal pH in *C. elegans*, that is, pH 5.5, *CalipHluor*$_{Ly}$ showed a K_d of 7.2 µM. As expected, the percentage signal change on chelating Ca^{2+} also decreases as acidity increases (Fig. 1d).

In vivo performance of *CalipHluor*. Next, we investigated the in vivo reporter characteristics of *CalipHluor*$_{Ly}$ as functions of lumenal pH and [Ca^{2+}]. When DNA-based reporters are injected into the pseudocoelom in *C. elegans*, they are specifically uptaken by coelomocytes through scavenger receptor-mediated endocytosis and thereby label organelles on the endolysosomal pathway[22,25]. After labeling endocytic organelles with *CalipHluor*$_{Ly}$, we clamped the lumenal pH and [Ca^{2+}] of coelomocytes. We achieved this by incubating worms in clamping buffers of fixed pH and [Ca^{2+}] containing nigericin, monensin, ionomycin, and ethylene glycol-bis(β-aminoethyl ether)-N,N,N',N'-tetraacetic acid (EGTA) at high [K^+], which clamped the endosomal ionic milieu to that of the surrounding buffer (Methods)[13,15,23,25]. Post-clamping, the worms were imaged in four channels: (1) the donor channel (donor or Alexa Fluor 488); (2) the FRET acceptor channel (acceptor), which corresponds to the intensity image of Alexa Fluor 647 fluorescence on exciation of Alexa Fluor 488; (3) the orange channel (O or Rhod-5F); and (4) the red channel (R), which corresponds to the intensity image of Alexa Fluor 647 fluorescence on directly exciting Alexa Fluor 647. Figure 2a shows representative images of a *CalipHluor*$_{Ly}$-labeled coelomocyte imaged in the four channels.

In a given clamping buffer of specified pH and Ca^{2+} concentration, the ratio of the donor channel image to the acceptor channel image yields a D/A image that corresponds to the clamping buffer pH (Fig. 2a). Similarly, the O/R image corresponds to the Ca^{2+} concentration at that pH (Fig. 2a). Representative D/A and O/R images of coelomocytes clamped at the indicated pH and [Ca^{2+}] are shown in Fig. 2b (Methods and Supplementary Fig. 3). The distribution of D/A and O/R values of lysosomes clamped at different indicated pH and [Ca^{2+}] values are shown in Fig. 2c,d. To compare the in vivo and in vitro sensing performances of both ion-sensing modules across a wide range of pH and Ca^{2+}, we plotted two parameters for each module in *CalipHluor*$_{Ly}$. For the pH-sensing module these were the fold change in D/A ($FC_{D/A}$) and the transition pH ($pH_{1/2}$) (Fig. 2e,f and Supplementary Fig. 4a–d). For the Ca^{2+}-sensing module, these were the fold change in O/R ($FC_{O/R}$) and the K_d for Ca^{2+} (Fig. 2g–j). The values of $FC_{D/A}$, $FC_{O/R}$, $pH_{1/2}$, and K_d in vivo and in vitro were consistent, revealing that the in vitro performance characteristics of *CalipHluor*$_{Ly}$ were quantitatively recapitulated in vivo (Fig. 2e,f,i,j).

Measuring [Ca^{2+}] in organelles of the endolysosomal pathway. Endosomal maturation, critical to both organelle function and cargo trafficking, is accompanied by progressive acidification of the organelle lumen (Fig. 3a)[32,33]. Unlike pH, little is known about lumenal Ca^{2+} changes as a function of endosomal maturation[16,17]. We therefore sought to demonstrate the applicability of our probe across a range of acidic organelles by mapping lumenal Ca^{2+} as a function of endosomal maturation. We determined the time points at which *CalipHluor*$_{Ly}$ localized in the early endosome, the late endosome, and the lysosome in coelomocytes as described previously[22] (Fig. 3b,c). Post-injection, *CalipHluor*$_{Ly}$ was found to localize

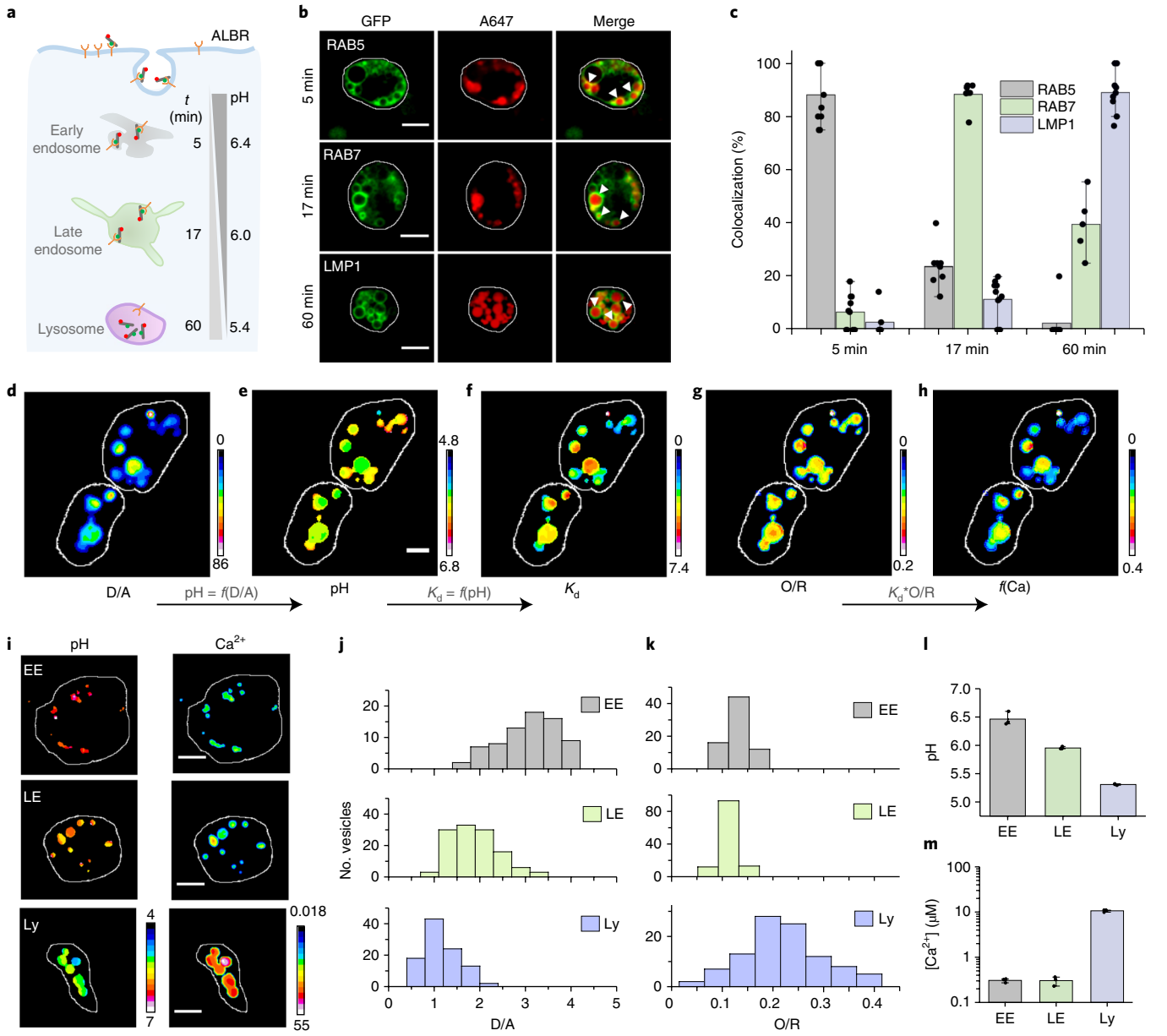

Fig. 3 | pH and [Ca²⁺] maps accompanying endosomal maturation. a, *CalipHluor* marks the indicated organelles in coelomocytes time-dependently, by scavenger receptor-mediated endocytosis. ALBR, anionic ligand-binding receptor. **b**, Colocalization of *CalipHluor* and GFP-tagged markers of endocytic organelles at indicated time points post-injection in nematodes. **c**, Quantification of colocalization in **b** ($n=10$ cells, ≥50 endosomes). **d**–**h**, Pseudocolor images of *CalipHluor*$_{Ly}$-labeled lysosomes where the D/A map (**d**) is converted to the corresponding pH map (**e**); the pH map is converted into a K_d map (**f**) where the value of K_d is encoded pixelwise according to the pH at that pixel; the K_d map (**f**) is multiplied by the O/R map (**g**) to yield the Ca^{2+} map (**h**). "*f*(*x*)" indicates the function of *x*. **i**, Representative pseudocolor pH and Ca^{2+} maps of early endosomes (EE), late endosomes (LE), and lysosomes (Ly) labeled with *CalipHluor and CalipHluor*$_{Ly}$. **j**,**k**, Distributions of D/A and O/R ratios of EE, LE, and Ly from $n=15$ cells, 50 endosomes. **l**, Mean endosomal pH of EE, LE, and Ly. **m**, Mean endosomal [Ca^{2+}] values in EE, LE, and Ly data represent the mean ± s.e.m. Experiments were repeated thrice independently with similar results.

in early endosomes, late endosomes, and lysosomes at 5, 17, and 60 min, respectively (Fig. 3b,c and Supplementary Fig. 5).

We measured pH and apparent Ca^{2+} at each stage in wild-type N2 nematodes with single-endosome addressability using our probes. We then incorporated a K_d correction factor for each endosome according to its measured pH, and then computed the true value of Ca^{2+} in every endosome. Figure 3d–h shows a representative set of coelomocytes for which this method of analysis was performed. We labeled early and late endosomes with *CalipHluor*, whereas we labeled lysosomes with the *CalipHluor*$_{Ly}$ variant, and then generated the D/A and O/R maps of coelomocytes (Methods and Fig. 3d–h).

The D/A map was directly converted into a pH map using the calibrated D/A values obtained from the in vivo pH clamping experiments (Fig. 3d–h and Supplementary Table 2). The in vivo and in vitro Ca^{2+} response characteristics at every pH (Fig. 2h) provide the K_d for Ca^{2+} at every pH value for both *CalipHluor* and *CalipHluor*$_{Ly}$.

Using the pH map in Fig. 3e, we constructed a 'K_d map' that corresponds to the K_d for Ca^{2+} at each pixel in the pH map (Fig. 3f and Methods). By multiplying the value of K_d at each pixel in the K_d map with the equation $(O/R-O/R_{min})/(O/R_{max}-O/R)$, we obtain the true Ca^{2+} map (Fig. 3h). In this equation, O/R corresponds to the observed O/R value at a given pixel in the O/R map, and O/R_{min}

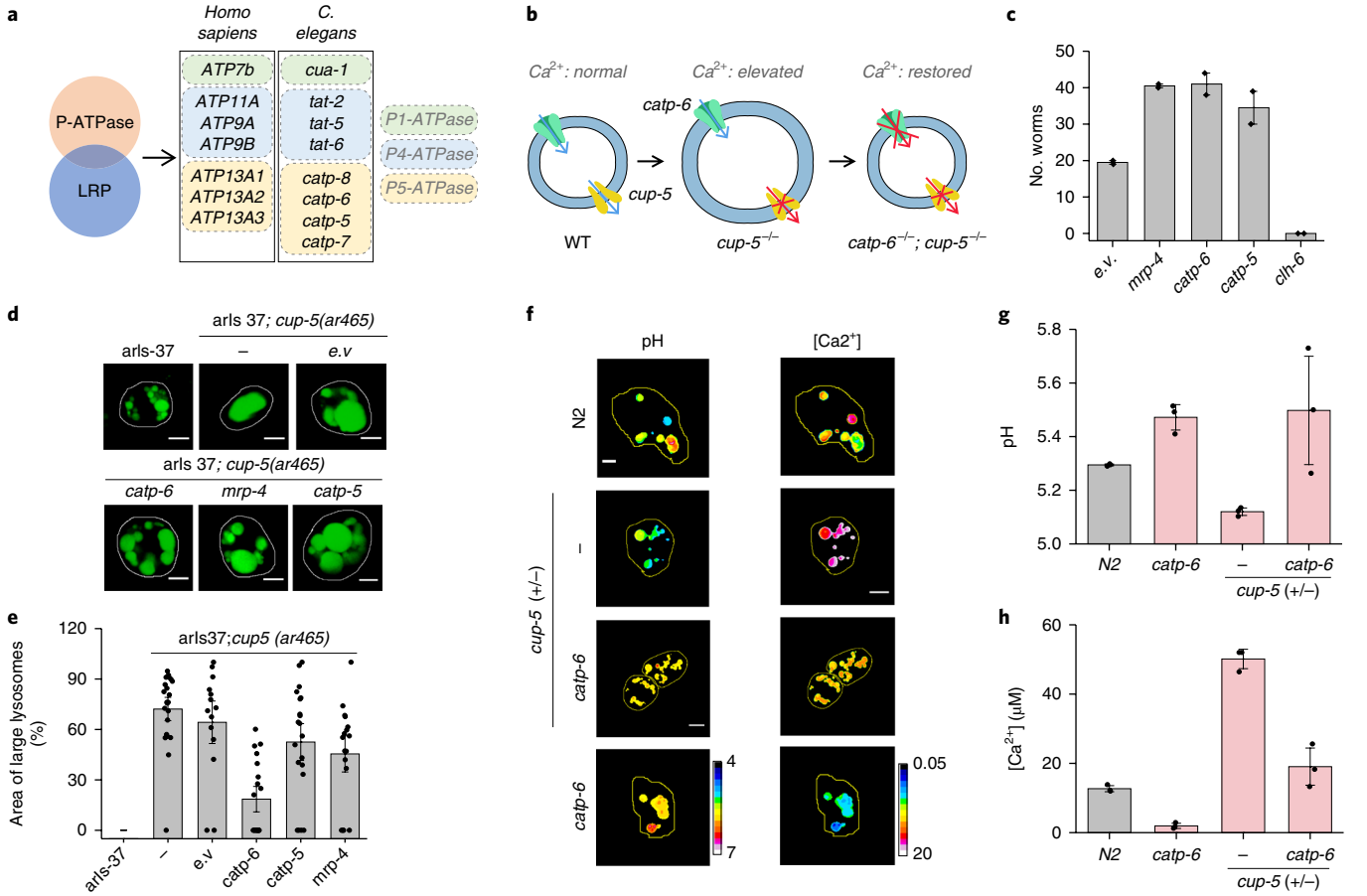

Fig. 4 | *Catp-6* facilitates lysosomal Ca^{2+} accumulation. a, P-type ATPases in human lysosomes obtained from the human Lysosome Gene Database. LRP, lysosome resident proteins. **b**, Functional connectivity between *catp-6* and *cup-5*. WT, wild type. **c**, Number of adult *cup-5*$^{+/-}$ progeny where the indicated proteins are knocked down by RNAi. Data represent mean ± s.e.m. of three independent trials. e.v., empty vector. **d**, Representative fluorescence images of *arls37[myo-3p::ssGFP+dpy-20 (+)]I* and *arls37; cup-5(ar465)* on RNAi knockdown of the indicated proteins. **e**, Percentage area occupied by enlarged lysosomes in the indicated genetic background. (n = 15 cells, ≥100 lysosomes). **f**, pH and Ca^{2+} maps in *CalipHluor*$_{Ly}$-labeled lysosomes in coelomocytes in indicated genetic backgrounds. N2, wild-type strain. **g**,**h**, Mean lysosomal pH (**g**) and mean lysosomal [Ca^{2+}] (**h**) in the indicated genetic backgrounds. Scale bar, 5 μm. Data represent mean ± s.e.m. Experiments were repeated thrice independently with similar results.

and O/R_{max} correspond to O/R values at 1 μM and 10 mM Ca^{2+} at the corresponding pH value at that particular pixel. We thus obtained pH and Ca^{2+} maps of early endosomes, late endosomes, and lysosomes in N2 worms (Fig. 3i) and the corresponding distributions of D/A and pH-corrected O/R are shown in Fig. 3j,k. The mean values of pH and Ca^{2+} in each endosomal stage are shown in Fig. 3l,m.

As expected, pH decreases progressively with endosomal maturation, with lumenal acidity showing an approximately threefold decrease at each endocytic stage. In contrast, Ca^{2+} in the early endosome and the late endosome were comparable and fairly low, that is, 0.3 μM. Interestingly, from the late endosome to the lysosome, lumenal Ca^{2+} increased sharply by ~35-fold, indicating a stage-specific enrichment of Ca^{2+} and consistent with the lysosome being an acidic Ca^{2+} store (Supplementary Table 3). The 100-fold difference between lysosomal and cytosolic Ca^{2+} is consistent with the stringent regulation of lysosomal Ca^{2+} channels to release lumenal Ca^{2+} and control lysosome function.

***Catp-6* is identified as a potential lysosomal Ca^{2+} importer.** This surge in lumenal Ca^{2+} specifically in the lysosome stage implicates the existence of factors that aid lysosomal import of Ca^{2+}. However, players that mediate lysosomal Ca^{2+} accumulation are still unknown in higher eukaryotes. We took inspiration from the well-known Ca^{2+} importer SERCA, a P-type ATPase that is present on the endoplasmic reticulum[26]. Other Ca^{2+} importers, such as plasma membrane Ca^{2+} ATPase and the secretory pathway Ca^{2+} ATPase (SPCA1), are also P-type ATPases[34]. Therefore, we manually identified potential P-type ATPases in the human lysosomal proteome[35–39]. We found that the P5 ATPase ATP13A2 was described to transport cations such as Mn^{2+}, Zn^{2+}, Mg^{2+}, and Cd^{2+}, but not Ca^{2+}, based on toxicity assays[27]. As Ca^{2+} homeostasis is critical to all major signaling pathways, compensatory mechanisms in cells can counter excess Ca^{2+} and thereby omit the identification of Ca^{2+} transport by ATP13A2.

C. elegans has two homologs of ATP13A2 *catp-5* and *catp-6* (Fig. 4a). To test whether *catp-6* mediated lysosomal Ca^{2+} accumulation, we investigated whether its knockdown would rescue a phenotype arising due to high lumenal Ca^{2+} (Fig. 4b). TRPML1 is a well-known lysosomal Ca^{2+} release channel whose knockdown would be expected to elevate lysosomal Ca^{2+} (refs [40,41]). Mutations in TRPML1 result in lysosomal dysfunction that leads to the lysosomal storage disease mucopolysaccharidoses type IV[42]. In *C. elegans*, loss of *cup-5*, the *C. elegans* homolog of TRPML1, results in lysosomal storage and embryonic lethality[43]. We therefore tested whether *catp-6* knockdown, in a *cup-5*$^{+/-}$ genetic background, could reverse *cup-5*$^{-/-}$ lethality. In this strain, the homozygous lethal deletion of *cup-5* is balanced by *dpy-10*-marked translocation[44]. We performed a survival assay by knocking down specific genes in *cup-5*$^{+/-}$ worms and scoring for lethality (Fig. 4c and Supplementary Fig. 6).

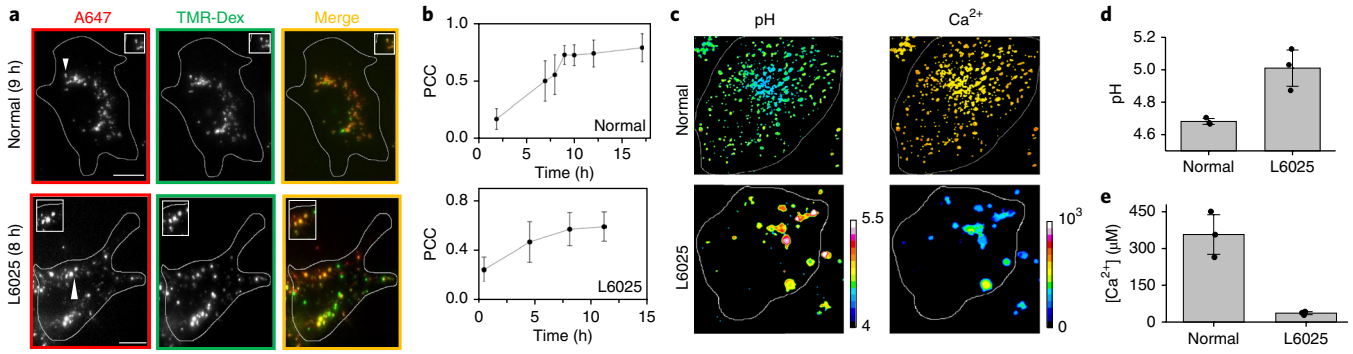

Fig. 5 | *CalipHluor*^{mLy} maps lysosomal Ca^{2+} in human cells. a, Representative images of lysosomes in fibroblast cells from healthy individuals and from subjects with Kufor–Rakeb syndrome (L6025) labeled with TMR-Dex (green) and *CalipHluor*^{mLy} (Alexa Fluor 647 (A647); red). **b**, Pearson correlation coefficient (PCC) of colocalization between *CalipHluor*^{mLy} and lysosomes as a function of time ($n = 20$ cells). **c**, Pseudocolor pH and Ca^{2+} maps of lysosomes in normal and L6025 fibroblasts. **d**,**e**, Mean lysosomal pH (**d**) and mean lysosomal [Ca^{2+}] (**e**) in normal and L6025 fibroblasts ($n = 5$ cells, 50 endosomes). Scale bar, 10 μm. Data represent mean ± s.e.m. Experiments were repeated thrice independently with similar results.

Multidrug resistance protein-4 (MRP-4) is a versatile efflux transporter for drugs, toxins, peptides, and lipids and is known to rescue *cup-5*$^{-/-}$ lethality[45]. It is hypothesized that in the absence of *cup-5*, *mrp-4* mis-localizes in endocytic compartments, causing toxicity that is then alleviated on its knockdown. RNA interference (RNAi) knockdown of either *catp-6* or *catp-5* rescued *cup-5*$^{-/-}$ lethality favorably compared with *mrp-4* knockdown (Supplementary Fig. 6). Knocking down *clh-6*, a gene encoding another lysosome-resident channel that regulates lumenal chloride, showed no such rescue[25,29].

***Catp-6* facilitates lysosomal Ca^{2+} accumulation.** Given that the rescue of lethality might occur without restoration of lysosomal function, we tested whether any of our candidate genes reversed lysosomal phenotypes. *Cup-5* knockdowns show abnormally large lysosomes due to lysosomal storage[29]. We therefore used the hypomorph *ar645* with a G401E mutation in *cup-5*, leading to dysfunction that is insufficient for lethality but that leads to engorged lysosomes[46]. In the *arIs37*;*cup-5(ar465)* strain, soluble green fluorescent protein (GFP) that is secreted from the muscle cells into the pseudocoelom is internalized by the coelomocytes and trafficked for degradation to dysfunctional lysosomes[46]. Thus, in these worms, the lysosomes in coelomocytes are abnormally enlarged and labeled with GFP (Fig. 4d).

RNAi knockdowns of *catp-6* in these nematodes rescued lysosomal morphology (Fig. 4d,e and Methods). Knocking down either *catp-5* or *mrp-4* showed only a marginal recovery of phenotype. The fact that the protein encoded by *mrp-4* is not lysosome-resident, combined with its inability to rescue the lysosomal phenotype, suggests that, mechanistically, its rescue of *cup-5*$^{-/-}$ lethality is likely to be extra-lysosomal, consistent with previous hypotheses.

We then checked whether *catp-6*-mediated rescue of a physical phenotype such as lysosome morphology also led to a restoration of a chemical phenotype, that is, its lumenal Ca^{2+}. Lysosomal Ca^{2+} measurements using *CalipHluor*$_{Ly}$ in *cup-5*$^{+/-}$ nematodes and in *catp-6* knockdowns were made. Wild-type nematodes showed lysosomal Ca^{2+} levels of 11 ± 0.8 μM (Fig. 4f–h). In *cup-5*$^{+/-}$ nematodes, lysosomal Ca^{2+} was elevated to 40 ± 1.5 μM, consistent with *cup-5* being a Ca^{2+} release channel (Fig. 4f–h). Interestingly, *catp-6* knockdown restored lysosomal Ca^{2+} to wild-type levels. Thus, *catp-6* function directly opposes that of *cup-5* as it rescues *cup-5*-deficient phenotypes at three levels—the whole organism in terms of lethality, the subcellular level in terms of lysosome phenotype, and the suborganelle level in terms of its lumenal chemical composition. Cumulatively, these indicate that *catp-6* facilitates lysosomal Ca^{2+} import. Accordingly, *catp-6* deletion led to lysosomal Ca^{2+} dropping to 1.6 ± 0.4 μM, consistent with it facilitating Ca^{2+} import.

ATP13A2 facilitates lysosomal Ca^{2+} accumulation. Mutations in ATP13A2, the human homolog of *catp-6*, belong to the PARK9 Parkinson's disease susceptibility locus. These mutations lead to the Kufor–Rakeb syndrome, a severe, early-onset, autosomal recessive form of Parkinson's disease with dementia[47]. Parkinson's disease is strongly connected to Ca^{2+} dysregulation because excessive cytosolic Ca^{2+} causes excitotoxicity of dopaminergic neurons[48]. Interestingly, overexpression of ATP13A2 suppresses toxicity and reduces cytosolic Ca^{2+} (refs [28,49]). Further, loss of ATP13A2 function leads to neuronal ceroid lipofuscinosis, a lysosomal storage disorder, thus implicating the lysosome as its potential site of action[50].

To confirm whether ATP13A2 also facilitates lysosomal Ca^{2+} import, we mapped lysosomal Ca^{2+} in human fibroblasts. We created a variant called *CalipHluor*^{mLy} suited to measure the high acidity of mammalian lysosomes (Supplementary Fig. 7a). *CalipHluor*^{mLy} showed similar pH and Ca^{2+} response characteristics in vitro, on beads, and *in cellulo*, and its Ca^{2+}-sensing characteristics are unaffected by the new pH-sensing module (Supplementary Fig. 7b–e)

We then localized *CalipHluor*^{mLy} in lysosomes of primary human dermal fibroblasts (HDF cells) obtained from punch-skin biopsies. We showed that *CalipHluor*^{mLy} labels lysosomes in skin fibroblasts by scavenger receptor-mediated endocytosis (Fig. 5a,b and Supplementary Fig. 8). Briefly, a 1-h pulse of 500 nM *CalipHluor*^{mLy} followed by a 9-h chase efficiently labeled lysosomes in this cell type (Fig. 5a,b).

We then measured lysosomal Ca^{2+} in fibroblasts from healthy individuals and L6025 primary fibroblasts isolated from male subjects with Kufor–Rakeb syndrome, which are homozygous for a C>T mutation in 1550 of ATP13A2[51]. This mutation results in ATP13A2 being unable to exit the endoplasmic reticulum, and the lysosomes are devoid of ATP13A2[51]. After confirming its lysosomal localization in L6025 cells, using *CalipHluor*^{mLy} we measured lysosomal pH and Ca^{2+} (Fig. 5b–e). Lysosomes from subjects with Kufor–Rakeb syndrome showed 14-fold lower [Ca^{2+}] and ~2-fold lower [H^+] than those from healthy individuals normal (Fig. 5c–e), confirming that ATP13A2 mediates lysosomal Ca^{2+} accumulation.

Discussion

Small-molecule and genetically encodable Ca^{2+} indicators have profoundly impacted biology. However, their pH sensitivity has restricted their use to the cytoplasm or the endoplasmic reticulum, where the pH is neutral and fairly constant. Ca^{2+} mapping of acidic microenvironments has therefore not been previously possible. Our DNA-based fluorescent reporter, *CalipHluor*, combines the photophysical advantages of small-molecule Ca^{2+} indicators with the precise organelle targetability of endocytic tracers. *CalipHluor* is a

pH-correctable Ca^{2+} reporter that simultaneously reports pH and Ca^{2+} in organelles, retaining concentration information on both ions with single-organelle addressability. Thus, by knowing exactly how the affinity (K_d) of the Ca^{2+}-sensitive probe changes with pH, we compute the K_d at every pixel in the pH map to generate a K_d map. From the K_d map and the O/R map, we can construct the true Ca^{2+} map of the acidic organelle.

Given the newfound ability to directly quantitate lysosomal Ca^{2+} using *CalipHluor*, we identified ATP13A2—a risk gene for Parkinson's disease—as a potential lysosomal Ca^{2+} importer. We found that the function of *catp-6*, the *C. elegans* homolog of ATP13A2, directly opposed that of a well-known lysosome-resident Ca^{2+} release channel, *cup-5*. It reversed *cup-5* phenotypes at three different levels—a whole-organism phenotype, a subcellular phenotype, and an intra-lysosomal phenotype. This now provides a framework to identify more lysosomal Ca^{2+} regulators.

The ability to map pH and Ca^{2+} with single-organelle addressability is critical to discriminate between lysosomal hypo-acidification and Ca^{2+} dysregulation. *CalipHluor* can be used to map lumenal Ca^{2+} changes in diverse organelles. There is already a range of DNA-based pH sensors specifically suited to organelles such as the Golgi, the recycling endosome, and the endoplasmic reticulum[20,21,23–25]. Given the array of small-molecule Ca^{2+} indicators covering various Ca^{2+} affinities, this positions *CalipHluor* technology to deliver new insights into organellar Ca^{2+} regulation.

Online content

Any methods, additional references, Nature Research reporting summaries, source data, statements of data availability and associated accession codes are available at https://doi.org/10.1038/s41592-018-0232-7.

Received: 21 June 2018; Accepted: 30 October 2018;
Published online: 10 December 2018

References

1. Clapham, D. E. Calcium signaling. *Cell* **131**, 1047–1058 (2007).
2. Bagur, R. & Hajnóczky, G. Intracellular Ca^{2+} sensing: its role in calcium homeostasis and signaling. *Mol. Cell* **66**, 780–788 (2017).
3. Yang, J., Zhao, Z., Gu, M., Feng, X. & Xu, H. Release and uptake mechanisms of vesicular Ca^{2+} stores. *Protein Cell* https://doi.org/10.1007/s13238-018-0523-x (2018).
4. Parenti, G., Andria, G. & Ballabio, A. Lysosomal storage diseases: from pathophysiology to therapy. *Annu. Rev. Med.* **66**, 471–486 (2015).
5. Plotegher, N. & Duchen, M. R. Crosstalk between lysosomes and mitochondria in Parkinson's disease. *Front. Cell Dev. Biol.* **5**, 110 (2017).
6. Xu, H., Martinoia, E. & Szabo, I. Organellar channels and transporters. *Cell Calcium* **58**, 1–10 (2015).
7. Calcraft, P. J. et al. NAADP mobilizes calcium from acidic organelles through two-pore channels. *Nature* **459**, 596–600 (2009).
8. Huang, P. et al. P2X4 forms functional ATP-activated cation channels on lysosomal membranes regulated by luminal pH. *J. Biol. Chem.* **289**, 17658–17667 (2014).
9. Kiselyov, K. et al. TRPML: transporters of metals in lysosomes essential for cell survival? *Cell Calcium* **50**, 288–294 (2011).
10. Lloyd-Evans, E. On the move, lysosomal CAX drives Ca^{2+} transport and motility. *J. Cell Biol.* **212**, 755–757 (2016).
11. Melchionda, M., Pittman, J. K., Mayor, R. & Patel, S. Ca^{2+}/H^{+} exchange by acidic organelles regulates cell migration in vivo. *J. Cell Biol.* **212**, 803–813 (2016).
12. Morgan, A. J., Davis, L. C. & Galione, A. Imaging approaches to measuring lysosomal calcium. *Methods Cell Biol.* **126**, 159–195 (2015).
13. Christensen, K. A., Myers, J. T. & Swanson, J. A. pH-dependent regulation of lysosomal calcium in macrophages. *J. Cell Sci.* **115**, 599–607 (2002).
14. Lloyd-Evans, E. et al. Niemann–Pick disease type C1 is a sphingosine storage disease that causes deregulation of lysosomal calcium. *Nat. Med.* **14**, 1247–1255 (2008).
15. Garrity, A. G. et al. The endoplasmic reticulum, not the pH gradient, drives calcium refilling of lysosomes. *eLife* **5**, e15887 (2016).
16. Sherwood, M. W. et al. Activation of trypsinogen in large endocytic vacuoles of pancreatic acinar cells. *Proc. Natl Acad. Sci. USA* **104**, 5674–5679 (2007).
17. Gerasimenko, J. V., Tepikin, A. V., Petersen, O. H. & Gerasimenko, O. V. Calcium uptake via endocytosis with rapid release from acidifying endosomes. *Curr. Biol.* **8**, 1335–1338 (1998).
18. Albrecht, T., Zhao, Y., Nguyen, T. H., Campbell, R. E. & Johnson, J. D. Fluorescent biosensors illuminate calcium levels within defined beta-cell endosome subpopulations. *Cell Calcium* **57**, 263–274 (2015).
19. Johnson, D. E., Ostrowski, P., Jaumouillé, V. & Grinstein, S. The position of lysosomes within the cell determines their luminal pH. *J. Cell Biol.* **212**, 677–692 (2016).
20. Chakraborty, K., Veetil, A. T., Jaffrey, S. R. & Krishnan, Y. Nucleic acid-based nanodevices in biological imaging. *Annu. Rev. Biochem.* **85**, 349–373 (2016).
21. Modi, S. et al. A DNA nanomachine that maps spatial and temporal pH changes inside living cells. *Nat. Nanotechnol.* **4**, 325–330 (2009).
22. Surana, S., Bhat, J. M., Koushika, S. P. & Krishnan, Y. An autonomous DNA nanomachine maps spatiotemporal pH changes in a multicellular living organism. *Nat. Commun.* **2**, 340 (2011).
23. Saha, S., Prakash, V., Halder, S., Chakraborty, K. & Krishnan, Y. A pH-independent DNA nanodevice for quantifying chloride transport in organelles of living cells. *Nat. Nanotechnol.* **10**, 645–651 (2015).
24. Modi, S., Nizak, C., Surana, S., Halder, S. & Krishnan, Y. Two DNA nanomachines map pH changes along intersecting endocytic pathways inside the same cell. *Nat. Nanotechnol.* **8**, 459–467 (2013).
25. Chakraborty, K., Leung, K. & Krishnan, Y. High lumenal chloride in the lysosome is critical for lysosome function. *eLife* **6**, e28862 (2017).
26. Toyoshima, C. & Inesi, G. Structural basis of ion pumping by Ca^{2+}-ATPase of the sarcoplasmic reticulum. *Annu. Rev. Biochem.* **73**, 269–292 (2004).
27. Schmidt, K., Wolfe, D. M., Stiller, B. & Pearce, D. A. Cd^{2+}, Mn^{2+}, Ni^{2+} and Se^{2+} toxicity to *Saccharomyces cerevisiae* lacking YPK9p the orthologue of human ATP13A2. *Biochem. Biophys. Res. Commun.* **383**, 198–202 (2009).
28. Ramonet, D. et al. PARK9-associated ATP13A2 localizes to intracellular acidic vesicles and regulates cation homeostasis and neuronal integrity. *Hum. Mol. Genet.* **21**, 1725–1743 (2012).
29. Fares, H. & Greenwald, I. Regulation of endocytosis by CUP-5, the *Caenorhabditis elegans* mucolipin-1 homolog. *Nat. Genet.* **28**, 64–68 (2001).
30. Salgado, E. N., Garcia Rodriguez, B., Narayanaswamy, N., Krishnan, Y. & Harrison, S. C. Visualization of Ca^{2+} loss from rotavirus during cell entry. *J. Virol.* https://doi.org/10.1128/JVI.01327–18 (2018).
31. Jewett, J. C., Sletten, E. M. & Bertozzi, C. R. Rapid Cu-free click chemistry with readily synthesized biarylazacyclooctynones. *J. Am. Chem. Soc.* **132**, 3688–3690 (2010).
32. Huotari, J. & Helenius, A. Endosome maturation. *EMBO J.* **30**, 3481–3500 (2011).
33. Hu, Y.-B., Dammer, E. B., Ren, R.-J. & Wang, G. The endosomal-lysosomal system: from acidification and cargo sorting to neurodegeneration. *Transl. Neurodegener.* **4**, 18 (2015).
34. Vandecaetsbeek, I., Vangheluwe, P., Raeymaekers, L., Wuytack, F. & Vanoevelen, J. The Ca^{2+} pumps of the endoplasmic reticulum and Golgi apparatus. *Cold Spring Harb. Perspect. Biol.* **3**, a004184 (2011).
35. Tharkeshwar, A. K. et al. A novel approach to analyze lysosomal dysfunctions through subcellular proteomics and lipidomics: the case of NPC1 deficiency. *Sci. Rep.* **7**, 41408 (2017).
36. Chapel, A. et al. An extended proteome map of the lysosomal membrane reveals novel potential transporters. *Mol. Cell. Proteomics* **12**, 1572–1588 (2013).
37. Lübke, T., Lobel, P. & Sleat, D. E. Proteomics of the lysosome. *Biochim. Biophys. Acta* **1793**, 625–635 (2009).
38. Brozzi, A., Urbanelli, L., Germain, P. L., Magini, A. & Emiliani, C. hLGDB: a database of human lysosomal genes and their regulation. *Database (Oxford)* **2013**, bat024 (2013).
39. Schröder, B. A., Wrocklage, C., Hasilik, A. & Saftig, P. The proteome of lysosomes. *Proteomics* **10**, 4053–4076 (2010).
40. Cao, Q., Yang, Y., Zhong, X. Z. & Dong, X.-P. The lysosomal Ca^{2+} release channel TRPML1 regulates lysosome size by activating calmodulin. *J. Biol. Chem.* **292**, 8424–8435 (2017).
41. Sahoo, N. et al. Gastric acid secretion from parietal cells is mediated by a Ca^{2+} efflux channel in the tubulovesicle. *Dev. Cell* **41**, 262–273 (2017).
42. Bargal, R. et al. Identification of the gene causing mucolipidosis type IV. *Nat. Genet.* **26**, 118–123 (2000).
43. Schaheen, L., Dang, H. & Fares, H. Basis of lethality in *C. elegans* lacking CUP-5, the mucolipidosis type IV orthologue. *Dev. Biol.* **293**, 382–391 (2006).
44. C. elegans Deletion Mutant Consortium. Large-scale screening for targeted knockouts in the *Caenorhabditis elegans* genome. *G3 (Bethesda)* **2**, 1415–1425 (2012).
45. Schaheen, L., Patton, G. & Fares, H. Suppression of the cup-5 mucolipidosis type IV-related lysosomal dysfunction by the inactivation of an ABC transporter in *C. elegans*. *Development* **133**, 3939–3948 (2006).
46. Fares, H. & Greenwald, I. Genetic analysis of endocytosis in *Caenorhabditis elegans*: coelomocyte uptake defective mutants. *Genetics* **159**, 133–145 (2001).

47. van Veen, S. et al. Cellular function and pathological role of ATP13A2 and related P-type transport ATPases in Parkinson's disease and other neurological disorders. *Front. Mol. Neurosci.* **7**, 48 (2014).
48. Schöndorf, D. C. et al. iPSC-derived neurons from GBA1-associated Parkinson's disease patients show autophagic defects and impaired calcium homeostasis. *Nat. Commun.* **5**, 4028 (2014).
49. Usenovic, M., Tresse, E., Mazzulli, J. R., Taylor, J. P. & Krainc, D. Deficiency of ATP13A2 leads to lysosomal dysfunction, α-synuclein accumulation, and neurotoxicity. *J. Neurosci.* **32**, 4240–4246 (2012).
50. Bras, J., Verloes, A., Schneider, S. A., Mole, S. E. & Guerreiro, R. J. Mutation of the parkinsonism gene ATP13A2 causes neuronal ceroid-lipofuscinosis. *Hum. Mol. Genet.* **21**, 2646–2650 (2012).
51. Estrada-Cuzcano, A. et al. Loss-of-function mutations in the ATP13A2/PARK9 gene cause complicated hereditary spastic paraplegia (SPG78). *Brain* **140**, 287–305 (2017).

Acknowledgements

We thank J. Kuriyan and M. Zajac for valuable comments. We thank the Integrated Light Microscopy facility at the University of Chicago, the Caenorhabditis Genetic Center for strains, and Ausubel Lab for Arhinger Library RNAi clones. We thank the Krainc lab at Northwestern University (Chicago, IL, USA) for the fibroblast cells harboring mutations in ATP13A2 (L6025). HDF cells were a kind gift from the lab of J. Rowley (University of Chicago, Chicago, IL, USA). This work was supported by the University of Chicago Women's Board; a Pilot and Feasibility award from an NIDDK center grant no. P30DK42086 to the University of Chicago Digestive Diseases Research Core Center; MRSEC grant no. DMR-1420709; the National Center for Advancing Translational Sciences of the National Institutes of Health through grant no. 1UL1TR002389-01 that funds the Institute for Translational Medicine, Chicago Biomedical Consortium, with support from the Searle Funds at The Chicago Community Trust, C-084; and University of Chicago start-up funds to Y.K. Y.K. is a Brain Research Foundation Fellow.

Author contributions

K.C. and Y.K. designed the project. N.N. synthesized and designed the calcium dye. N.N., K.C., A.S., E.Z., and K.L. performed experiments. J.D. provided key resources. N.N., K.C., A.S., and Y.K. analyzed the data. K.C. and Y.K wrote the paper. All authors discussed the results and gave inputs on the manuscript.

Competing interests

The authors declare no competing interests.

Additional information

Supplementary information is available for this paper at https://doi.org/10.1038/s41592-018-0232-7.

Reprints and permissions information is available at www.nature.com/reprints.

Correspondence and requests for materials should be addressed to K.C. or Y.K.

Publisher's note: Springer Nature remains neutral with regard to jurisdictional claims in published maps and institutional affiliations.

Methods

Preparation of BAPTA-5F aldehyde (1). BAPTA-5F aldehyde (1) was synthesized according to a previously reported procedure[52,53]. $POCl_3$ (1.12 g, 7.3 mmol) was added to DMF (5 ml) at 0 °C and stirred for 10 min. After 10 min, BAPTA-5F (1.6 g, 2.9 mmol) in DMF (3 ml) was added to the above solution and heated to 65 °C. After completion of the reaction, the reaction mixture was poured into water and the pH was adjusted to 6.0 by aqueous NaOH (1 M) solution. Product was extracted with ethylacetate (3 × 50 ml) and solvent was evaporated. Crude product was purified by column chromatography on silica gel using hexane/EtOAc (70%/30% to 60%/40%) as an eluent to obtain BAPTA-5F aldehyde (1) in 65% yield. ^{1}H-NMR (500 MHz, $CDCl_3$) δ_{ppm} 9.80 (s, 1H), 7.30–7.45 (m, 2H), 6.83 (t, 1H, J = 7 Hz), 6.76 (d, 1H, J = 8 Hz), 6.59 (t, 2H, J = 8 Hz), 4.40 (t, 2H, J = 7.0 Hz), 4.35 (t, 2H, J = 7.5 Hz), 4.33 (s, 4H), 4.22 (s, 4H), 3.59 (s, 6H), 3.57 (s, 6H). ^{13}C-NMR (125 MHz, $CDCl_3$) δ_{ppm} 190.5, 171.8, 171.2, 159.4, 157.5, 151.4, 151.3, 149.6, 145.1, 135.6, 135.5, 130.0, 126.9, 120.3, 120.2, 116.6, 110.8, 107.3, 107.1, 101.3, 101.1, 67.1, 67.0, 53.5, 53.4, 51.9, 51.7. High-resolution mass spectrometry (HRMS) electrospray ionization (ESI) m/z: M^+ calculated for $C_{27}H_{31}FN_2O_{11}^+$ 578.1912, found: 578.1927.

Synthesis of Rhod-5F. Schemes showing the synthesis of compounds described in this paper are presented in Supplementary Note 1.

To a solution of BAPTA-5F aldehyde (1) (50 mg, 0.086 mmol) in propionic acid (4 ml), 3-(dimethylamino) phenol (26 mg, 0.19 mmol) and *p*-toluenesulfonic acid (1.5 mg, 0.009 mmol) were added and the mixture was stirred at room temperature for 12 h. After 12 h, chloranil (21 mg, 0.086 mmol) in dichloromethane (DCM) (3 ml) was added to the above reaction mixture and then stirred at room temperature overnight. After completion of the reaction, the crude product was extracted with DCM (3 × 30 ml). The crude product was then purified by column chromatography on silica gel using DCM/methanol (95%/5% to 90%/10%) as an eluent to obtain methyl ester of Rhod-5F as a dark red solid in 35% yield. Liquid chromatography mass spectrometry (LCMS) (ESI) m/z: M^+ calculated for $C_{43}H_{48}FN_4O_{11}^+$ 815.3298, found: 815.5. Methyl ester of Rhod-5F (5 mg, 0.006 mmol) was dissolved in a methanol and water mixture (1:0.5 ml), to which KOH (3.5 mg, 0.063 mmol) was added and stirred for 8 h at room temperature. After completion of the reaction, the solution pH was adjusted to 6.0 and crude product was extracted with DCM (3 × 5 ml). Product was purified by HPLC (50:50 acetonitrile/water, 0.1% TFA) to obtained Rhod-5F. LCMS (ESI) m/z: M^+ calculated for $C_{39}H_{40}FN_4O_{11}^+$ 759.2672, found: 759.4.

Preparation of 1-azido-3-iodopropane (2). To a solution of 1-bromo-3-chloropropane (1 g, 6.4 mmol) in dimethylsulfoxide (DMSO) (8 ml), sodium azide (0.5 g, 7.7 mmol) was added and stirred at room temperature for 12 h. After completion of the reaction, the mixture was diluted with water and the product was extracted with hexane to obtain 1-azido-3-chloropropane. Sodium iodide (1.5 g, 10 mmol) was then added to a solution of 1-azido-3-chloropropane (1 g, 8.4 mmol) in acetone (25 ml) and stirred at room temperature for 8 h. After completion of the reaction, the solvent was evaporated under vacuum. The crude product was diluted with a saturated solution of $Na_2S_2O_3$ to quench the unreacted iodine, followed by extraction of the compound with ethyl acetate (3 × 50 ml). This was dried over Na_2SO_4 and the product, 1-azido-3-iodopropane (2), was used for further reactions without purification.

Preparation of 3-((3-azidopropyl)(methyl)amino)phenol (3). To a solution of 3-aminophenol (1 g, 9.2 mmol) in acetone (30 ml), potassium carbonate (2.5 g, 18.4 mmol) was added and stirred at room temperature for 20 min. After 20 min, iodomethane (1.3 g, 9.2 mmol) was added and the mixture was further stirred for 8 h at room temperature. After completion of reaction, the solvent was evaporated and the crude product was extracted with DCM (3 × 30 ml). This was followed by purification of the crude product by column chromatography on silica gel using hexane/ethyl acetate (80%/20%) as an eluent to obtain 3-(methylamino) phenol in 45% yield.

To a solution of 3-(methylamino) phenol (1 g, 8.1 mmol) in DMF (8 ml), N,N-diisopropylethylamine (1.26 g, 9.7 mmol) was added and stirred for 20 min at room temperature. After 20 min, 1-azido-3-iodopropane (2) (1.7 g, 8.1 mmol) was added to the above reaction mixture and heated at 65 °C for 8 h. After completion of the reaction, the solvent was evaporated and the crude product was extracted with diethylether (3 × 40 ml). Then, the crude product was purified by column chromatography on silica gel using hexane/ethyl acetate (90%/10%) as an eluent to obtain 3-((3-azidopropyl)(methyl)amino)phenol (3) liquid in 72% yield. ^{1}H-NMR (500 MHz, $CDCl_3$) δ_{ppm} 7.09–7.13 (m, 1H), 6.3 (d, 1H, J = 7.5 Hz), 6.21 (dd, 2H, J = 2 Hz, 8.5 Hz), 3.42 (t, 2H, J = 6.5 Hz), 3.38 (t, 2H, J = 7 Hz), 2.94 (s, 3H), 1.87 (t, 2H, J = 6.5 Hz). ^{13}C-NMR (125 MHz, $CDCl_3$) δ_{ppm} 156.7, 150.7, 130.2, 105.1, 103.5, 99.3, 49.8, 49.2, 38.6, 26.3. HRMS (ESI) m/z: M^+ calculated for $C_{10}H_{14}N_4O^+$ 206.1168, found: 206.1177.

Preparation of Rhod-5F-OMe (4). To a solution of BAPTA-5F aldehyde (1) (50 mg, 0.086 mmol) in propionic acid (4 ml), 3-((3-azidopropyl)(methyl)amino) phenol (3) (40 mg, 0.19 mmol) and *p*-toluenesulfonic acid (1.5 mg, 0.009 mmol) were added and stirred at room temperature for 12 h. After 12 h, chloranil (21 mg, 0.086 mmol) in DCM (3 ml) was added to above reaction mixture and stirred at room temperature overnight. After completion of the reaction, the solvent was evaporated and the crude product was extracted with DCM (3 × 20 ml). The crude product was then purified by column chromatography on silica gel using DCM/methanol (95%/5% to 90%/10%) as an eluent to obtain Rhod-5F-OMe (4) as a dark red solid in 30% yield. ^{1}H-NMR (500 MHz, DMSO-d_6) δ_{ppm} 7.55 (d, 2H, J = 8 Hz), 7.15–7.16 (m, 3H), 7.00–7.04 (m, 3H), 6.88 (dd, 2H, J = 3 Hz, 9 Hz), 6.75 (dd, 1H, J = 6 Hz, 9 Hz), 6.65 (td, 1H, J = 3 Hz, 6 Hz), 4.20–4.30 (m, 8H), 4.02 (s, 4H), 3.71 (t, 4H, J = 7 Hz), 3.53 (s, 6H), 3.47 (s, 10H), 3.25 (s, 6H), 1.88 (q, 4H, J = 7 Hz). ^{13}C-NMR (125 MHz, DMSO-d_6) δ_{ppm} 171.2, 171.1, 158.3, 157.3, 156.4, 156.1, 140.7, 135.2, 135.1, 131.9, 123.6, 123.1, 119.1, 116.8, 114.9, 114.4, 106.4, 106.2, 101.2, 101.0, 96.4, 67.3, 67.2, 54.9, 53.2, 53.0, 51.5, 51.2, 49.7, 48.6, 48.1, 26.0, 22.1. HRMS (ESI) m/z: M^+ calculated for $C_{47}H_{54}FN_{10}O_{11}^+$ 953.3952, found: 953.3967.

Preparation of Rhod-5F-N_3. Rhod-5F-OMe (4) (5 mg, 0.005 mmol) was dissolved in a methanol and water mixture (1:0.5 ml), to which KOH (3.5 mg, 0.063 mmol) was added and stirred for 8 h at room temperature. After completion of the reaction, the solution pH was adjusted to 6.0 and crude product was extracted with DCM (3 × 5 ml). Product was purified by HPLC (50:50 acetonitrile/water, 0.1% TFA). LCMS (ESI) m/z: M^+ calculated for $C_{43}H_{46}FN_{10}O_{11}^+$ 897.3326, found: 897.5.

Reagents. All of the chemicals used for the synthesis of Rhod-5F-N_3 were purchased from Sigma and Alfa Aesar. ^{1}H-NMR and ^{13}C-NMR were recorded on a Bruker AVANCE II+ 500 MHz NMR spectrophotometer in $CDCl_3$ and DMSO-d_6 and tetramethylsilane used as an internal standard. Mass spectra were recorded using an Agilent 6224 Accurate-Mass TOF LC/MS instrument.

All fluorescently labeled oligonucleotides were purchased from IDT and IBA-GmBh. HPLC-purified oligonucleotides were dissolved in Milli-Q water to make 100 µM stock solutions and quantified using an ultraviolet spectrophotometer and stored at −20 °C. EGTA, ampicillin, carbencillin, isopropyl β-D-1-thiogalactopyranoside, nigericin, and monensin were purchased from Sigma, and ionomycin was obtained from Cayman Chemical. Maleylated BSA (mBSA) was maleylated according to a previously published protocol[21]. Monodisperse silica microspheres were obtained from Cospheric.

Rhod-5F conjugation and sample preparation. Rhod-5F was first conjugated to D2 and O3-DBCO strands. Rhod-5F-N_3 (25 µM) was added to 5 µM DBCO-labeled D2 strand in 100 µl of sodium phosphate (10 mM) buffer containing KCl (100 mM) at pH 7.0 and stirred overnight at room temperature. After completion of the reaction, 10 µl of 3 M sodium acetate (pH 5.5) and 250 µl of ethanol were added to the reaction mixture and kept overnight at −20 °C for DNA precipitation[54]. Then, the reaction mixture was centrifuged at 14,000 r.p.m. at 4 °C for 20 min to remove the unreacted Rhod-5F-N_3 and the precipitate was resuspended in ethanol and centrifuged. This procedure was repeated three times for complete removal of unreacted Rhod-5F-N_3. Rhod-5F conjugation was confirmed by gel electrophoresis on a native polyacrylamide gel containing 15% (19:1 acrylamide/bis-acrylaimde) in 1× buffer of Tris-HCl (100 mM), boric acid (89 mM), and EDTA (2 mM), pH 8.3. The same protocol was used for the conjugation of Rhod-5F-N_3 to O3-DBCO.

To prepare a *CalipHluor*$_{Ly}$ and *CalipHluor*^{mLy} sample, we mixed 5 µM D1 or OG-D1 and 5 µM Rhod-5F-conjugated D2 strands in equimolar ratios in 10 mM sodium phosphate buffer (pH 7.2) containing 100 mM KCl. The resultant solution was heated to 90 °C for 15 min, cooled to room temperature at 5 °C per 15 min, and kept at 4 °C overnight[21]. For *CalipHluor*, 5 µM O1-A488, 5 µM O2-A647, and 5 µM Rhod-5F-conjugated O3 strands were mixed in equimolar ratios in 10 mM sodium phosphate buffer at pH 5.5 containing 100 mM KCl. The solution was heated to 90 °C for 15 min, then cooled to room temperature at 3 °C per 15 min and kept at 4 °C overnight. See Supplementary Table 1 for sequence information.

In vitro fluorescence measurements. Fluorescence spectra were measured on a FluoroMax-4 spectrophotometer (Horiba Scientific) using previously established protocols[21]. For in vitro pH measurements, a *CalipHluor*$_{Ly}$ sample was diluted to 30 nM in a pH clamping buffer ($CaCl_2$ (50 µM to 10 mM), HEPES (10 mM), MES (10 mM), sodium acetate (10 mM), EGTA (10 mM), KCl (140 mM), NaCl (5 mM), and $MgCl_2$ (1 mM)) of the desired pH and equilibrated for 30 min at room temperature. All of the samples were excited at 495 nm and emission spectra were collected from 505 nm to 750 nm. The ratio of donor emission intensity at 520 nm to acceptor emission intensity at 665 nm was plotted as a function of pH to generate the pH calibration curve. Means of D/A from two independent experiments and their s.e.m. values were plotted for each pH. $FC_{D/A}$ of *CalipHluor*$_{Ly}$ was calculated from the ratios of D/A at pH 4.0 and pH 6.5. $pH_{1/2}$ values for *CalipHluor*$_{Ly}$ at different [Ca^{2+}] values were derived from a pH calibration curve by fitting to a Boltzmann sigmoid.

For in vitro [Ca^{2+}] measurements, a *CalipHluor*$_{Ly}$ sample was diluted to 30 nM in Ca^{2+} clamping buffer (HEPES (10 mM), MES (10 mM), sodium acetate (10 mM), EGTA (10 mM), KCl (140 mM), NaCl (5 mM), and $MgCl_2$ (1 mM)). We then varied the [Ca^{2+}] from 0 mM to 20 mM and adjusted to different pH values (4.5–7.2). The free [Ca^{2+}] at a given pH was calculated based on Maxchelator software (http://maxchelator.stanford.edu/). Rhod-5F and Alexa Fluor 647 were excited at 545 nm

and 630 nm, respectively. Emission spectra for Rhod-5F (O) and Alexa Fluor 647 (R) were collected from 570–620 nm and 660–750 nm, respectively. Means of O/R from two independent experiments and their s.e.m. values were plotted for each $[Ca^{2+}]$. Similar experiments were performed with 50 nM *CalipHluor*^{mLy} at pH 4.6 and pH 5.1. We obtained the in vitro calcium binding affinity (K_d) of Rhod-5F by plotting ratios of Rhod-5F (O) emission intensity at 580 nm to Alexa Fluor 647 (R) emission intensity at 665 nm as a function of free $[Ca^{2+}]$ and fitted them using a sigmoidal growth Hill equation:

$$Y = S + (E - S) \times (X^n / (K_d^n + X^n)) \quad (1)$$

where X is the free $[Ca^{2+}]$, Y is the O/R ratio at given free $[Ca^{2+}]$, S is the O/R ratio at low $[Ca^{2+}]$, E is the O/R ratio at high $[Ca^{2+}]$, and n is the Hill coefficient. Fold change response in O/R of *CalipHluor*$_{Ly}$ was calculated from ratio of O/R at high $[Ca^{2+}]$ and O/R at low $[Ca^{2+}]$.

***C. elegans* methods and strains.** Standard methods were followed for the maintenance of *C. elegans*[55]. The wild-type strain used was the *C. elegans* isolate from Bristol, strain N2 (Brenner, 1974). Strains used in the study, provided by the Caenorhabditis Genetics Center, are RRID:WB-STRAIN:RB2510 W08D2.5(ok3473) and RRID:WBSTRAIN:VC1242 *[+/mT1 II; cup-5(ok1698)/mT1 [dpy-10(e128)] III*]. Transgenics used in this study, also provided by the Caenorhabditis Genetics Center, are RRID:WB-STRAIN:NP1129 *cdIs131 [pcc1::GFP::rab-5+unc-119(+)+myo-2p::GFP]*, a transgenic strain that expresses GFP-fused early endosomal marker RAB-5 inside coelomocytes; RRID:WB-STRAIN:NP871 *cdIs66 [pcc1::GFP::rab-7+unc-119(+)+myo-2p::GFP]*, a transgenic strain that expresses GFP-fused late endosomal/lysosomal marker RAB-7 inside coelomocytes; RRID:WB-STRAIN:RT258 *pwIs50 [lmp-1::GFP+Cbr-unc-119(+)]*, a transgenic strain expressing GFP-tagged lysosomal marker LMP-1; *arIs37[myo-3p::ssGFP+dpy-20(+)]I*, a transgenic strain that expresses soluble GFP (ssGFP) in the body muscles, which is secreted in pseudocoelom and endocytosed by coelomocytes; and *arIs37[myo-3p::ssGFP+dpy-20(+)]Icup5(ar465)*, a transgenic strain with enlarged GFP-containing vesicles in coelomocytes due to defective degradation. Gene knockdown was performed using Ahringer Library-based RNAi methods[56]. The RNAi clones used were L4440 empty vector control, *catp-6* (W08D2.5, Ahringer Library), *catp-5* (K07E3.7, Ahringer Library), and *mrp-4* (F21G4.2, Ahringer Library).

***CalipHluor* trafficking in coelomocytes.** *CalipHluor* trafficking in coelomocytes was done in transgenic strains expressing endosomal markers such as GFP::RAB-5 (early endosomes), GFP::RAB-7 (late endosomes), and LMP-1::GFP (lysosomes), as described previously by our laboratory[22]. Briefly, worms were injected with *CalipHluor*$_{A647}$ (500 nM) and incubated for specific amounts of time then transferred onto ice. Worms were anesthetized using 40 mM sodium azide in M9 solution. Worms were then imaged on a Leica TCS SP5 II STED laser scanning confocal microscope (Leica Microsystems, Inc.) using an Argon ion laser for 488-nm excitation and an He-Ne laser for 633-nm excitation, with a set of filters suitable for GFP and Alexa Fluor 647, respectively. We determined colocalization of GFP and *CalipHluor*$_{A647}$ by counting the number of *CalipHluor*$_{A647}$-positive puncta that colocalized with GFP-positive puncta and quantifying it as a percentage of the total number of *CalipHluor*$_{A647}$-positive puncta[22]. To confirm lysosomal labeling in a given genetic background, the same procedure was performed on the relevant mutant or RNAi knockdown in *pwIs50 [lmp-1::GFP+Cb-unc-119(+)]*.

RNAi experiments. Bacteria from the Ahringer RNAi library expressing double-stranded RNA against the relevant gene were fed to worms, and measurements were carried out in 1-d-old adults of the F1 progeny[56]. RNA knockdown was confirmed by probing messenger RNA levels of the candidate gene, assayed by RT–PCR. Briefly, total RNA was isolated using the Trizol-chloroform method; 2.5 µg total RNA was converted to complementary DNA using oligo-dT primers. Then, 5 µl of the reverse transcription (RT) reaction was used to set up a PCR using gene-specific primers. Actin mRNA was used as a control. PCR products were separated on a 1.5% agarose-Tris base, acetic acid and EDTA (TAE) gel.

Image acquisition. Image acquisition was carried out on a wide-field IX83 inverted microscope (Olympus Corporation of the Americas) using a 60×/1.42-NA (numerical aperture) phase contrast oil-immersion objective (PLAPON, Olympus Corporation of the Americas) and an Evolve Delta 512 EMCCD (electron-multiplying charge-coupled device) camera (Photometrics). Filter wheel, shutter, and CCD (charge-coupled device) camera were controlled using Metamorph Premier Ver 7.8.12.0 (Molecular Devices), suitable for the fluorophores used. Images on the same day were acquired under the same acquisition settings. Alexa Fluor 488 channel images (donor) were obtained using a 480/20 band-pass excitation filter, a 520/40 band-pass emission filter, and an 89016-ET-FITC/Cy3/Cy5 dichroic filter. Alexa Fluor 647 channel images (acceptor) were obtained using a 640/30 band-pass excitation filter, a 705/72 band-pass emission filter, and an 89016-ET-FITC/Cy3/Cy5 dichroic filter. FRET channel images were obtained using the 480/20 band-pass excitation filter, 705/72 band-pass emission filter, and 89016-ET-FITC/Cy3/Cy5 dichroic filter. Rhod-5F channel images (O) were obtained using a 545/25 band-pass excitation filter, a 595/50 band-pass emission filter, and a an 89016-ET-FITC/Cy3/Cy5 dichroic filter. Confocal images were acquired on a Leica TCS SP5 II STED laser scanning confocal microscope (Leica Microsystems) equipped with a 63×/1.4-NA oil-immersion objective. Alexa Fluor 488 was excited using an argon ion laser for 488-nm excitation, Alexa Fluor 647 using an He-Ne laser for 633-nm excitation, and Rhod-5F using a laser for 561-nm excitation with a set of dichroic, excitation, and emission filters suitable for each fluorophore.

Image analysis. Image analysis for quantification of pH and calcium in single endosomes was done using custom MATLAB code. For each cell the most focused plane was manually selected in the Alexa Fluor 647 channel. This image and corresponding images from the same z-position in other channels were input into the program. Images from the different channels were then aligned using enhanced cross-correlation optimization[57]. To determine the location of the endosome, first a low threshold was used to select the entire cell. Only the area within the cell was subsequently considered for endosome selection. Regions of interest corresponding to individual endosomes were selected in the Alexa Fluor 647 channel by adaptive thresholding using Sauvola's method[58]. The initial selection was further refined by watershed segmentation and size filtering. After segmentation, regions of interest were inspected in each image and selection errors were corrected manually. Using the cell boundary, an annular region 10 pixels wide around the cell was selected and used to calculate a background intensity in each image. Then, we measured the mean fluorescence intensity in each endosome in donor, acceptor, Rhod-5F (O), and Alexa Fluor 647 (R) channels, and the background intensity corresponding to that cell and channel was subtracted. The two ratios of intensities (D/A and O/R) were then computed for each endosome. Mean D/A of each distribution was plotted as a function of pH to obtain the in vivo pH calibration curve. Mean O/R of each distribution was plotted as a function of free $[Ca^{2+}]$ to generate the in vivo Ca^{2+} calibration curve. Pseudocolor pH and Ca^{2+} images were obtained by measuring the D/A and O/R ratios per pixel, respectively.

In vivo measurements of pH and $[Ca^{2+}]$. In vivo pH calibration experiments of *CalipHluor*$_{Ly}$ were carried out using protocols previously established in our laboratory[21,22]. Briefly, *CalipHluor*$_{Ly}$ (500 nM) was microinjected in the pseudocoelom of young adult worms on the opposite side of the vulva. After microinjections, worms were incubated at 22 °C for 2 h for maximum labeling of coelomocyte lysosomes. Then, worms were immersed in clamping buffer ($CaCl_2$ (50 µM to 10 mM), HEPES (10 mM), MES (10 mM), sodium acetate (10 mM), EGTA (10 mM), KCl (140 mM), NaCl (5 mM), and $MgCl_2$ (1 mM)) of the desired pH containing the ionophores nigericin (50 µM), monensin (50 µM), and ionomycin (20 µM). Worm cuticle was perforated to facilitate the entry of buffer into the body. After 75 min of incubation in clamping buffer, coelomocytes were imaged using wide-field microscopy. Three independent measurements, each with ten worms, were made for each pH value.

Ca^{2+} clamping measurements were carried out using *CalipHluor*$_{Ly}$. Worms were injected with *CalipHluor*$_{Ly}$ (500 nM) and incubated at 22 °C for 2 h. After 2 h, worms were immersed in Ca^{2+} clamping buffer (HEPES (10 mM), MES (10 mM), sodium acetate (10 mM), EGTA (10 mM), KCl (140 mM), NaCl (5 mM), and $MgCl_2$ (1 mM)) with varying amounts of free $[Ca^{2+}]$ from 1 µM to 10 mM and different pH values (5.3–6.5). Three independent measurements, each with ten worms, were made for Ca^{2+} value.

Early-endosome and late-endosome pH and free $[Ca^{2+}]$ measurements were carried out using *CalipHluor*, and lysosomal pH and free $[Ca^{2+}]$ measurements were carried out using *CalipHluor*$_{Ly}$. For real-time pH and $[Ca^{2+}]$ measurements, ten hermaphrodites were injected with 500 nM *CalipHluor* and *CalipHluor*$_{Ly}$ for early endosomes, late endosomes, and lysosomes, respectively, and incubated for the indicated time points (early endosomes, 5 min; late endosomes, 17 min; and lysosomes, 60 min). Worms were anesthetized with 40 mM sodium azide in M9 solution and imaged by wide-field microscopy. Image analysis was carried out with custom MATLAB code as described for image analysis.

Calculating pH-corrected $[Ca^{2+}]$ in early endosomes, late endosomes, and lysosomes. The D/A and O/R ratios in lysosomes, late endosomes, and early endosomes were measured using *CalipHluor*$_{Ly}$ and *CalipHluor* as mentioned above at single-endosome resolution. Over 100 endosomes were analyzed in each measurement in worms to generate a Gaussian spread of D/A. Around 5% of endosomes fell outside the range of mean ± 2 s.d., which was set as a threshold for our measurements in early endosomes, late endosomes, and lysosomes. To get pH-corrected $[Ca^{2+}]$ values, we measured the pH value in each individual endosome with single-endosome resolution from their D/A ratios. pH values in endosomes were calculated using equation (2), which was derived from our in vivo pH calibration curve.

$$\mathrm{pH} = \mathrm{pH}_{1/2} + \left[0.3 \ln\left(\left(\frac{K_1 - K_2}{Y - K_2}\right) - 1\right)\right] \quad (2)$$

where K_1, K_2, and $pH_{1/2}$ represent parameters from a Boltzmann fit of the in vivo pH calibration curve, and Y represents the D/A ratio in a given endosome.

Next, the K_d of *CalipHluor*$_{Ly}$ and fold-change response in O/R ratios of *CalipHluor*$_{Ly}$ from low [Ca^{2+}] O/R to high [Ca^{2+}] were obtained as functions of pH. We measured the in vitro and in vivo K_d values at different pH points ranging from 4.5 to 7.2 by fitting Ca^{2+} calibration curves by fitting to the Hill equation (1). From in vitro and in vivo [Ca^{2+}] calibration curves, the K_d of *CalipHluor*$_{Ly}$ was plotted as a function of pH using the following equation:

$$K_d = 1.03 + 5.14 \times 10^{12} \times e^{(-\mathrm{pH}/0.189)} + 3.108 \times 10^{6} \times e^{(-\mathrm{pH}/0.412)} \quad (3)$$

By using equation (3), we can deduce K_d of *CalipHluor*$_{Ly}$ at any given pH in early endosomes, late endosomes, and lysosomes. We obtained O/R_{max} (that is, the O/R ratio at high [Ca^{2+}]) by clamping the worms at 10 mM free [Ca^{2+}] at different pH points. In vitro and in vivo [Ca^{2+}] calibration curves showed that *CalipHluor*$_{Ly}$ retained its fold-change response of O/R from 1 µM to 10 mM at different pH points. O/R_{min} (that is, O/R ratio at low [Ca^{2+}]) values were calculated from fold-change response as a function of pH and normalized to O/R_{max}.

$$O/R_{min} = \frac{1}{4.24 + 0.12 \times \exp(0.5 \times \mathrm{pH})} \quad (4)$$

As mentioned above, the pH in early endosomes, late endosomes, and lysosomes was measured from D/A via equation (2) at single-endosome resolution. pH and O/R were used to calculate K_d and O/R_{min} from equations (3) and (4). Finally, K_d, O/R_{min}, O/R, and O/R_{max} were substituted in the following equation to get pH-corrected free [Ca^{2+}] values in endosomes by endosome level:

$$\mathrm{Free}[Ca^{2+}] = K_d \times \left[\frac{O/R - O/R_{min}}{O/R_{max} - O/R}\right] \quad (5)$$

Three independent measurements, each with ten worms, were made for pH and [Ca^{2+}] values in early endosomes, late endosomes, and lysosomes.

Image analysis—pH-corrected [Ca^{2+}] images. High-resolution images were acquired using confocal microscopy as mentioned earlier in the Methods. Images were acquired in four channels (Alexa Fluor 488, FRET, Rhod-5F, and Alexa Fluor 647) to quantify pH and [Ca^{2+}] at single-endosome resolution. To compensate for the pH component in Ca^{2+} measurements, the K_d of *CalipHluor*$_{Ly}$ at single endolysosomal compartments was calculated based on the K_d calibration plot discussed above. We quantified the pH of endolysosomes by measuring the donor/acceptor values calibrated across physiological pH (4.0–6.5). We background-subtracted donor and acceptor images by drawing a region of interest outside the worms. The donor image was duplicated and a threshold was set to create a binary mask. Background-subtracted donor and acceptor images were then multiplied with the binary mask to get processed donor and acceptor images. This processed donor image was divided by the processed acceptor image to get a pseudocolor D/A image, using the Image Calculator module of ImageJ[59]. The pH value was calculated via equation (2) formulated from an in vivo and in vitro pH calibration plot.

The pseudocolored pH image was processed to get a K_d image as shown in Fig. 3. K_d of *CalipHluor*$_{Ly}$ is a function of pH and this relation is formulated by the K_d calibration plot in vivo and in vitro using equation (3). For image processing of pH image to K_d image, background was set to a non-zero value. The K_d image represents the affinity of *CalipHluor*$_{Ly}$ for calcium and thus compensating the calcium image (O/R) with K_d would precisely represent the calcium levels at single endolysosomes. The pH-dependent K_d compensation was performed according to equation (5), where O/R_{max} and O/R_{min} were calculated by incubating CalipHluor-coated beads at 10 mM and 1 µM, respectively. Image calculations were done using the Image Calculator module in ImageJ. This image was multiplied with the binary image to bring the background value to zero. The pH-corrected K_d images were obtained for various mutants for accurate comparison of calcium levels in lysosomes.

Survival assay. *+/mT1 II; cup-5(ok1698)/mT1 [dpy-10(e128)] III* nematode strain was used for this assay[44]. Homozygous lethal deletion of *cup-5* gene is balanced by *dpy-10*-marked translocation. Heterozygotes are superficially wild type [*cup5*+/−], *Dpys* (mT1 homozygotes) are sterile, and *cup-5(ok1698)* homozygotes are lethal. *cup5*$^{+/-}$ L4 worms were placed on plates containing RNAi bacterial strains for L4440 empty vector (positive control), *mrp-4*, *catp-6*, *catp-5*, and *clh-6*. These worms were allowed to grow for 24 h and lay eggs, after which the adult worms were removed from the plates. The eggs were allowed to hatch and grow into adults for 3 d. The worm plates were then imaged under an Olympus SZX-Zb12 Research Stereomicroscope (Olympus Corporation of the Americas) with a Zeiss Axiocam color CCD camera (Carl Zeiss Microscopy). The images were analyzed using ImageJ software to count the number of adult worms per plate. Three independent plates were used for each RNAi background.

Lysosomal size recovery assay. *arIs37 [myo-3p::ssGFP+dpy-20(+)] I. cup-5(ar465)* is a transgenic nematode strain that secretes GFP from the body muscle cells, and this is endocytosed by coelomocytes which show enlarged GFP-labeled vesicles as a result of defective degradation caused by *cup 5* mutation[29]. Similar to the previous assay, *arIs37*; *cup-5(ar465)* L4 worms were placed on plates containing RNAi bacterial strains for empty vector (control), *catp-6, catp-5*, and *mrp-4* (positive control). The worms lay eggs for 24 h after which they are removed from the plates. The eggs hatch and the larvae grow to adulthood, after which they are imaged to check for lysosomal size differences. Worms were imaged on a Leica TCS SP5 II STED laser scanning confocal microscope (Leica Microsystems) equipped with a 63×/1.4-NA oil-immersion objective on excitation with an argon laser in the Alexa Fluor 488 channel. Lysosomal areas were measured using ImageJ. Of 100 lysosomes in *arIs37* worms, 7 lysosomes had an area in the range of 7.0–9.5 µm^2. Enlarged lysosomes are defined as those lysosomes whose diameter is ≥33% of the diameter of the largest lysosome observed in normal N2 worms. We measured the lysosomal area in *arIs37*; *cup-5(ar465)* worms in various RNAi bacteria-containing plates. Lysosomal size recovery data were plotted as the percentage of area occupied by large lysosomes relative to the total lysosomal area ($n = 15$ cells, >100 lysosomes).

Bead calibration of *CalipHluor*^{mLy}. Bead calibration was performed using *CalipHluor*^{mLy}-coated 0.6-µm monodisperse silica microspheres (Cospheric). Briefly, silica microspheres were incubated in a solution of 5 µM *CalipHluor*^{mLy} in 20 mM sodium acetate buffer (pH 5.1) and 500 mM NaCl for 1 h[60,61]. This binding solution was then spun down and the beads were reconstituted in clamping buffer (HEPES (10 mM), MES (10 mM), sodium acetate (10 mM), EGTA (10 mM), KCl (140 mM), NaCl (500 mM), and $MgCl_2$ (1 mM)). We then varied the [Ca^{2+}] from ~0 mM to 10 mM and adjusted the pH to either pH 4.6 or pH 5.1. The beads were incubated in clamping buffer for 30 min, after which there were imaged on a slide on the IX83 inverted microscope in the green channel (G) for Oregon Green, orange channel (O) for Rhod-5F, and red channel (R) for Alexa Fluor 647 to obtain G/R (pH) and O/R (Ca^{2+}) images.

Cell culture methods and maintenance. HDF cells were a kind gift from the late Professor Janet Rowley's laboratory at the University of Chicago, and human fibroblast cells harboring mutations in ATP13A2 (L6025) were a kind gift from the Krainc Laboratory, Northwestern University, Chicago. L6025 is homozygous for 1550 C>T. Control and mutant fibroblasts were cultured in DMEM (Invitrogen) containing 10% heat-inactivated fetal bovine serum (Invitrogen), 100 U ml^{-1} penicillin, and 100 µg ml^{-1} streptomycin and maintained at 37 °C under 5% CO_2.

Competition experiments in cells. HDF cells were washed with 1× PBS buffer pH 7.4, before labeling. Cells were incubated with 10 µM mBSA or BSA for 15 min and pulsed with media containing 500 nM *CalipHluor*^{mLy} and 10 µM mBSA or BSA for 1 h to allow internalization by receptor-mediated endocytosis, washed 3 times with 1× PBS, and then imaged under a wide-field microscope. Whole-cell intensities in the Alexa Fluor 647 channel were quantified for >30 cells per dish. The mean intensity values from three different experiments were normalized with respect to the autofluorescence and presented as the fraction internalized.

Colocalization in cells. We used lysosomes prelabeled with 10 kDa tetramethylrhodamine-dextran (TMR-Dex) to study the trafficking time scales for our probes. TMR-Dex was pulsed for 1 h, then chased for 16 h in fibroblast cells followed by imaging. Prelabeled cells were pulsed with 500 nM *CalipHluor*$_{A647Ly}$, then chased for the indicated time and imaged. Cross-talk and bleed-through were measured and found to be negligible between the TMR channel and the Alexa Fluor 647 channel. Pearson's correlation coefficient (PCC) measures the pixel-by-pixel covariance in the signal levels of two images. Tools for quantifying PCC are provided in Fuji software.

***In cellulo* measurements—pH and calcium measurements.** pH and calcium clamping were carried out using *CalipHluor*^{mLy}. Fibroblast cells were pulsed for 1 h and chased for 2 h with 500 nM *CalipHluor*^{mLy}. Cells were then fixed with 200 ml of 4% paraformaldehyde for 15 min at room temperature, washed 3 times, and retained in 1× PBS. To obtain the intracellular pH and calcium calibration profile, endosomal calcium concentrations were equalized by incubating the previously fixed cells in the appropriate calcium clamping buffer (HEPES (10 mM), MES (10 mM), sodium acetate (10 mM), EGTA (10 mM), KCl (140 mM), NaCl (5 mM), and $MgCl_2$ (1 mM)) by varying the amount of free [Ca^{2+}] from 1 µM to 10 mM and adjusting to different pH values. The buffer also contained nigericin (50 µM), monensin (50 µM), and ionomycin (20 µM) and the cells were incubated for 2 h at room temperature.

For real-time pH and calcium measurements, fibroblast cells were pulsed with 500 nM *CalipHluor*^{mLy} for 1 h, chased for 9 h (8 h for L0625 cells), and then washed with 1× PBS and imaged in Hank's balanced salt solution. Imaging was carried out on an IX83 research inverted microscope (Olympus Corporation of the Americas) using a 100×/1.42-NA oil-immersion objective (PLAPON, Olympus Corporation of the Americas) and an Evolve Delta 512 EMCCD camera (Photometrics).

Reporting Summary. Further information on research design is available in the Nature Research Reporting Summary linked to this article.

Data availability

The data that support the plots within this paper and the findings of this study are available from the corresponding author upon reasonable request.

References

52. Grynkiewicz, G., Poenie, M. & Tsien, R. Y. A new generation of Ca^{2+} indicators with greatly improved fluorescence properties. *J. Biol. Chem.* **260**, 3440–3450 (1985).
53. Collot, M. et al. CaRuby-Nano: a novel high affinity calcium probe for dual color imaging. *eLife* **4**, e05808 (2015).
54. Moore, D. & Dowhan, D. Purification and concentration of DNA from aqueous solutions. *Curr. Protoc. Mol. Biol.* **59**, 2.1.1–2.1.10 (2002).
55. Brenner, S. The genetics of *Caenorhabditis elegans*. *Genetics* **77**, 71–94 (1974).
56. Kamath, R. S. & Ahringer, J. Genome-wide RNAi screening in *Caenorhabditis elegans*. *Methods* **30**, 313–321 (2003).
57. Evangelidis, G. D. & Psarakis, E. Z. Parametric image alignment using enhanced correlation coefficient maximization. *IEEE Trans. Pattern Anal. Mach. Intell.* **30**, 1858–1865 (2008).
58. Sauvola, J. & Pietikäinen, M. Adaptive document image binarization. *Pattern Recognit.* **33**, 225–236 (2000).
59. Schindelin, J. et al. Fiji: an open-source platform for biological-image analysis. *Nat. Methods* **9**, 676–682 (2012).
60. Engelstein, M. et al. An efficient, automatable template preparation for high throughput sequencing. *Microb. Comp. Genomics* **3**, 237–241 (1998).
61. Vandeventer, P. E. et al. Multiphasic DNA adsorption to silica surfaces under varying buffer, pH, and ionic strength conditions. *J. Phys. Chem. B* **116**, 5661–5670 (2012).

nature research

Corresponding author(s): Kasturi Chakraborty and Yamuna Krishnan

Reporting Summary

Nature Research wishes to improve the reproducibility of the work that we publish. This form provides structure for consistency and transparency in reporting. For further information on Nature Research policies, see Authors & Referees and the Editorial Policy Checklist.

Statistical parameters

When statistical analyses are reported, confirm that the following items are present in the relevant location (e.g. figure legend, table legend, main text, or Methods section).

n/a	Confirmed	
☐	☒	The exact sample size (*n*) for each experimental group/condition, given as a discrete number and unit of measurement
☐	☒	An indication of whether measurements were taken from distinct samples or whether the same sample was measured repeatedly
☒	☐	The statistical test(s) used AND whether they are one- or two-sided *Only common tests should be described solely by name; describe more complex techniques in the Methods section.*
☒	☐	A description of all covariates tested
☐	☒	A description of any assumptions or corrections, such as tests of normality and adjustment for multiple comparisons
☐	☒	A full description of the statistics including central tendency (e.g. means) or other basic estimates (e.g. regression coefficient) AND variation (e.g. standard deviation) or associated estimates of uncertainty (e.g. confidence intervals)
☒	☐	For null hypothesis testing, the test statistic (e.g. *F*, *t*, *r*) with confidence intervals, effect sizes, degrees of freedom and *P* value noted *Give P values as exact values whenever suitable.*
☒	☐	For Bayesian analysis, information on the choice of priors and Markov chain Monte Carlo settings
☒	☐	For hierarchical and complex designs, identification of the appropriate level for tests and full reporting of outcomes
☒	☐	Estimates of effect sizes (e.g. Cohen's *d*, Pearson's *r*), indicating how they were calculated
☐	☒	Clearly defined error bars *State explicitly what error bars represent (e.g. SD, SE, CI)*

Our web collection on statistics for biologists may be useful.

Software and code

Policy information about availability of computer code

Data collection	Metamorph Premier ver 7.8.12.0 (Molecular Devices, LLC, USA) for image acquisition, FluorEssence ver 6.5 for fluorescence measurements, Image Lab™ Software 6.0.0 for PAGE image acquisition Section: Online methods.
Data analysis	Origin 2018 b9.4.0.220 (OriginLab Corporation, Northampton, MA, USA) for data plotting, ImageJ/Fiji 1.52e and Matlab R2017a(9.2.0.538062) for image analysis Section: Online methods.

For manuscripts utilizing custom algorithms or software that are central to the research but not yet described in published literature, software must be made available to editors/reviewers upon request. We strongly encourage code deposition in a community repository (e.g. GitHub). See the Nature Research guidelines for submitting code & software for further information.

Data

Policy information about availability of data

All manuscripts must include a data availability statement. This statement should provide the following information, where applicable:

- Accession codes, unique identifiers, or web links for publicly available datasets
- A list of figures that have associated raw data
- A description of any restrictions on data availability

The raw data that supports all the figures in this paper and other findings of this study are available from the corresponding author upon reasonable request.

Field-specific reporting

Please select the best fit for your research. If you are not sure, read the appropriate sections before making your selection.

☒ Life sciences ☐ Behavioural & social sciences ☐ Ecological, evolutionary & environmental sciences

For a reference copy of the document with all sections, see nature.com/authors/policies/ReportingSummary-flat.pdf

Life sciences study design

All studies must disclose on these points even when the disclosure is negative.

Sample size	Sample size was determined based on adequate representation of the population. Replicates were performed to ensure reproducibility.
Data exclusions	No data were excluded from the analyses.
Replication	In vitro and on beads fluorescence characterization assays and gels were all performed independently in duplicates. pH and calcium calibration and real time imaging, worm lethality assay and lysosomal size assays were performed in triplicates to ensure reproducibility. All replications were successful.
Randomization	Allocation was random. NGM plates containing various worm strains were randomized for selection in imaging experiments and biochemical assays.
Blinding	We used DNA based quantitative imaging technology to compare calcium and pH levels under different genetic conditions. Thus, it was not necessary to design a blinding group allocation.

Reporting for specific materials, systems and methods

Materials & experimental systems

n/a	Involved in the study
☐	☒ Unique biological materials
☒	☐ Antibodies
☒	☐ Eukaryotic cell lines
☒	☐ Palaeontology
☐	☒ Animals and other organisms
☒	☐ Human research participants

Methods

n/a	Involved in the study
☒	☐ ChIP-seq
☒	☐ Flow cytometry
☒	☐ MRI-based neuroimaging

Unique biological materials

Policy information about availability of materials

Obtaining unique materials	Various versions of the DNA sensors are readily available from the authors or from IDT/IBALifesciences.Human dermal fibroblasts (HDF) were a kind gift from Late Professor Janet Rowley's Lab at the University of Chicago and human fibroblast cells harboring mutations in ATP13A2 (L6025) were a kind gift from Krainc Lab, Northwestern University, Chicago. C.elegans strains were obtained from Caenorhabditis Genetic Center.

Animals and other organisms

Policy information about studies involving animals; ARRIVE guidelines recommended for reporting animal research

Laboratory animals	C.elegans strains were obtained from Caenorhabditis Genetic Center. All clamping, pH and calcium measurements were performed in one day old hermaphrodite adult worms. Details of all worm strains used are provided in the Online methods under the section "C.elegans methods and strains"
Wild animals	No wild animals were used in this study
Field-collected samples	Study did not involve samples collected from the field